Available online at www.sciencedirect.com

ScienceDirect

Geochimica et Cosmochimica Acta 285 (2020) 175–192

Geochimica et Cosmochimica Acta

www.elsevier.com/locate/gca

Lithium isotope behavior in Hawaiian regoliths: Soil-atmosphere-biosphere exchanges

Wenshuai Li [a,*], Xiao-Ming Liu [a,b,*], Oliver A. Chadwick [c]

[a] Department of Geological Sciences, University of North Carolina-Chapel Hill, NC, USA
[b] State Key Laboratory of Marine Geology, Tongji University, Shanghai, China
[c] Department of Geography, University of California, Santa Barbara, CA, USA

Received 20 September 2019; accepted in revised form 7 July 2020; available online 16 July 2020

Abstract

Understanding the influence of terrestrial soil-atmosphere-biosphere exchanges on Li geochemical behaviors is vital before using Li isotopes as a weathering tracer. We investigated Li geochemistry of the humid and arid regolith profiles formed on the Pololu lavas, the Kohala Mountain, Hawaii. The shallow regolith (0–1 m depth) retains Li ($\tau_{Li,Nb} > 0$) and displays peak Li accumulation in biologically-active, near-surface soil layers (humid, $\tau_{Li,Nb} = 10.9$; arid, $\tau_{Li,Nb} = 2.8$), with heavy Li isotopic compositions (humid, 4.7–9.9‰; arid, 4.0–13.9‰) with respect to the basalt signal (2.2‰). The deep regolith (>1 m) demonstrates δ^7Li (ave. 3.3‰) comparable to the composition of the underlying parent basalt (2.2‰). Decoupling of Li abundance and isotopic composition in the shallow regolith from those of the deep regolith implies different regolith controls on Li chemistry at vertical locations. The Li geochemistry in the shallow regolith has been substantially influenced by: (i) atmospheric deposition, (ii) plant cycling, and (iii) secondary mineral formation. In addition to weathering alteration, our data show that dust addition mainly influences δ^7Li in the humid regolith, and marine aerosol largely affects δ^7Li in the arid regolith. In the humid regolith, downward seepage migration allows for deeper and more advanced weathering, whereas occasional wetting events followed by rapid drying likely dominate in the arid regolith. Thus, biological cycling and the deposition of Asian dust and volcanic ash from the more recent Hawi eruptions are responsible for upward Li enrichment in soils and increases of soil δ^7Li composition in the shallow regolith. This is particularly important in the humid site with dense plant coverage and heavy rainfall. By contrast, the deep regolith of the humid and arid sites is mostly affected by pore fluid percolation and accumulation, thus inheriting heavy Li isotope signals from pore fluids. Our study emphasizes climate-regulated and long-neglected biological controls on terrestrial Li cycling during chemical weathering.

Keywords: Lithium isotopes; Hawaii; Regolith; Chemical weathering; Biogeochemistry

1. INTRODUCTION

Chemical weathering is one of the primary sinks of atmospheric carbon dioxide over geological timescales, modulating Earth climate and habitability (e.g., Gaillardet et al., 1999; Kump et al., 2000; Kasting and Catling, 2003; Beaulieu et al., 2012; Li and West, 2014). Its significance in controlling the evolution of continent-ocean-atmosphere systems has stimulated the development of multiple geochemical proxies to understand weathering history (e.g., Kamber et al., 2005; Pogge von Strandmann et al., 2013; Vigier and Goddéris, 2015; Bataille et al., 2017). In particular, the isotope fractionations of light elements (Li, Mg, Ca, and Si, etc.) during chemical weathering

* Corresponding authors at: Department of Geological Sciences, University of North Carolina-Chapel Hill, NC, USA (X.-M. Liu).
E-mail addresses: wenshuai@ad.unc.edu (W. Li), xiaomliu@e-mail.unc.edu (X.-M. Liu).

https://doi.org/10.1016/j.gca.2020.07.012
0016-7037/

provides valuable information on Earth's climate evolution and nutrient supplies from continents to oceans (e.g., Georg et al., 2007; Blättler et al., 2011; Li and West, 2014; Liu et al., 2013, 2014; Pogge von Strandmann and Henderson, 2015).

The lithium (Li) isotope system appears to be an ideal proxy for tracing silicate weathering (Tomascak, 2004) because the two stable isotopes (^{6}Li and ^{7}Li) have large relative mass difference (~17%), producing considerable isotope fractionation on Earth's surface (up to 60‰, Penniston-Dorland et al., 2017). Unlike bio-essential nutrients such as Ca, Si and Mg, Li is not considered to be an important component in the biosphere, because of (i) its non-micronutrient nature (Pogge von Strandmann et al., 2012), (ii) low concentrations of Li in biomass, and (iii) unsystematic isotope fractionation between plant tissues and in plant-soil systems (e.g., Lemarchand et al., 2010; Clergue et al., 2015). Furthermore, Li has only one redox state (+1), so it is insensitive to redox changes. In addition, the riverine Li isotope budget is dominated by weathering of silicate rocks, even in carbonate-dominated catchments due to its high abundance in silicate rocks compared to their carbonate counterparts (Tomascak, 2004). During chemical weathering, ^{6}Li is preferentially sequestered into secondary minerals; therefore, Li isotopic signatures preserved in weathering products could be quantitatively related to weathering intensities, rates or regimes (e.g., Vigier et al., 2008, 2009; Millot et al., 2010a; Pogge von Strandmann and Henderson, 2015; Hindshaw et al., 2019; Murphy et al., 2019). Commonly, the Li isotopic signals preserved in marine carbonates offer key information on silicate weathering over Earth's history (Liu and Rudnick, 2011; Misra and Froelich, 2012).

Recently, weathering-driven Li isotope fractionation in Earth's surface environments has received great attention (see review in Penniston-Dorland et al., 2017). Geological δ^7Li records have been examined to interpret: (i) Li budget balances between riverine inputs and submarine reverse weathering outputs (Misra and Froelich, 2012), (ii) oceanic Li isotope mass balance influenced by global weathering regimes (Li and West, 2014), (iii) Li isotope fractionation between soils and waters produced by modern chemical weathering (Pistiner and Henderson, 2003; Kisakürek et al., 2004; Wanner et al., 2014), and (iv) eolian imprints on soil Li isotopic signatures (Lemarchand et al., 2010; Liu et al., 2013; Ryu et al., 2014). Broadly, weathering of terrestrial rocks leaves an isotopically light regolith, balancing the heavy Li isotope reservoirs in rivers and oceans. Previous studies have demonstrated a wide δ^7Li range of weathering products retained in the regolith, which may be complicated by soil formation, pore-fluid advection/diffusion, and atmospheric inputs (marine aerosol and dust) (Huh et al., 2004; Teng et al., 2010; Liu et al., 2013). However, Li accumulation or depletion and the isotopic signals in the regolith are complex, and the interpretation of regolith Li records is not well constrained (Fig. S1). In addition, the key controls under different climate conditions may vary largely.

In this study, we compared the processes of soil-atmosphere-biosphere exchanges for Li isotope fractionation in regolith profiles developed on same-age lavas in humid and arid climatic conditions in the Kohala Mountain, Hawaii. Previous work on Hawaiian soils along a humid chronosequence with ~2500 mm·a^{-1} annual rainfall (Ryu et al., 2014) and a 150-ka climosequence (Huh et al., 2004) documented Li isotopic responses to weathering mass budgets and atmospheric inputs. However, these studies mainly focused on solid-phase regolith and less on potential biological or aqueous influences. Hence, we conducted a systematic biogeochemical investigation on regolith profiles, plants, and groundwater and river waters to understand potential influences on Li isotope geochemistry. We sampled two ~350 ka regolith profiles previously studied by Goodfellow et al. (2014). They developed under contrasting climatic conditions with mean annual rainfall (MAP) of 385 ± 53 mm·a^{-1} (arid, PO) and 1730 ± 57 mm·a^{-1} (humid, BE) (Giambelluca et al., 2013). In addition to Li and radiogenic Sr isotope analysis of bulk soils, we used operationally defined sequential extraction methods to determine the Li isotopic compositions in different soil compartments. We also measured the Li isotopic compositions of bulk plants and plant tissues to understand the controls of biological activities on Li geochemistry. Lastly, we estimated Li input and output fluxes of the regolith using a mass balance box model, and addressed broader implications.

2. GEOLOGICAL OVERVIEW

The Kohala Mountain is the northwestern-most and oldest volcano making up Hawaii Island. It has a strong windward - leeward contrast in rainfall, which is useful for evaluating the climatic impacts on chemical weathering over long time scales (Chadwick et al., 2003). There are two chemically distinct surface lavas exposed on the Kohala Mountain: the Pololu volcanics that are composed mainly of tholeiitic basalts ~350 ka in age, and the Hawi lavas that form an alkalic cap over the central part of the mountain ~150 ka in age (Spengler and Garcia, 1988; Chadwick et al., 2003). We sampled the profiles on minimally eroded locations on the Pololu flows and assume that the radiometric age of the lava flows is equivalent to the duration of weathering (~350 ka). We evaluated the behavior of Li isotopes in the arid (PO) and humid (BE) regoliths, which have been characterized in detail by Goodfellow et al. (2014) (Fig. 1).

The humid profile (BE) is located in the roadcut along the Highway 270 in the vicinity of the Bond Estate site (20.228843, −155.78962; MAP: $1{,}730 \pm 57$ mm) covered with pasture grasses and macadamia nut trees, and the arid profile (PO) is located in another roadcut along the same highway between Mahukona and Kaiwaihae (20.135715, −155.8859; MAP: 385 ± 53 mm) covered with sparse pasture grass (e.g., Porder et al., 2007; Giambelluca et al., 2013). The exposed portion of the humid regolith is approximately 15 m vertically, which has been sub-divided into 13 vertically distributed units according to texture, color, hardness, and fracture spacing, etc. (Goodfellow et al., 2014). We sampled the upper five regolith units from a backhoe pit reaching from the surface to 350 cm depth.

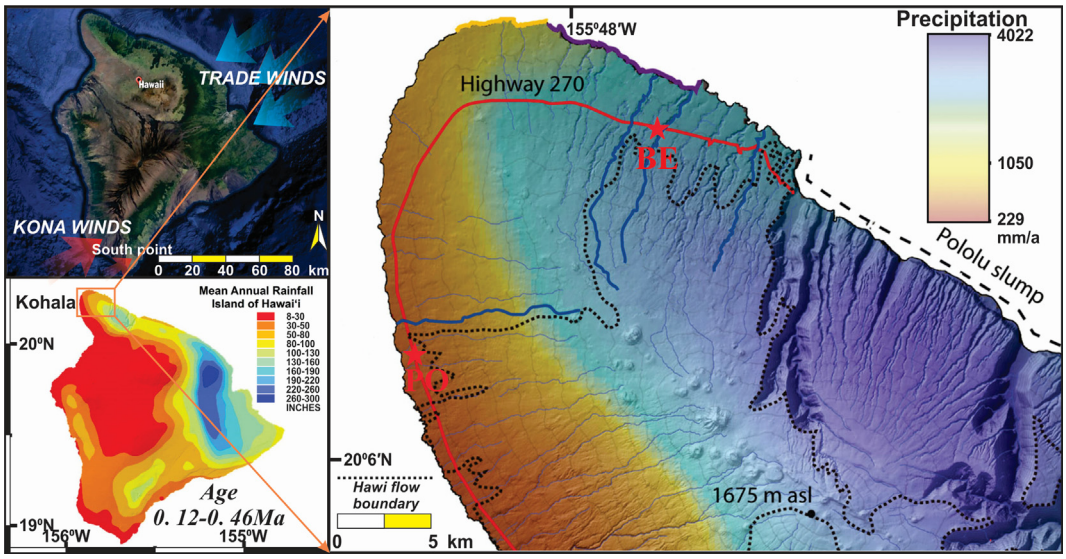

Fig. 1. Maps showing the location, geomorphology, and climate of the humid (BE) and arid (PO) regolith profiles on the Pololu flow (~350 ka), see description in Goodfellow et al. (2014). Due to critical orographic effects, moisture-bearing Trade Wind and Kona Wind deliver heavy precipitation to the NE flank and the south point of the island. The substrate ages are provided by Chadwick et al. (1999), and the mean annual precipitation (MAP) refers to Giambelluca et al. (2013) and 2011 Rainfall Atlas of Hawaii by the Department of Geography of University of Hawaii at Mānoa.

The arid road-cut exposure has a thickness of ~3.5 m, which can be divided into 5 units in a vertical order. The top 1 m is strongly weathered, whereas the rock is minimally weathered in the 1 to 2 m depth range, and below, there is little evidence of weathering except along fractures in the rock. Detailed physicochemical characterizations, including field observation, X-ray fluorescence analysis, digital terrain analysis, and division, are provided by Goodfellow et al. (2014).

In response to rainfall differences and its associated long-term water balance, the two studied regolith profiles exhibit differences in mineral weathering, elemental losses, and weathering depth. On an annual basis, local water balance (precipitation vs. evapotranspiration) is slightly positive in the humid regolith but highly negative in the arid regolith. The humid regolith is strongly weathering because of strong water infiltration, while the arid regolith experienced moderate weathering in the near surface (<1m) and little weathering below 1 m. To assess Li geochemical behaviors and regolith processes, we used the term "shallow regolith" to refer to horizons < 1 m deep, and "deep regolith" >1 m deep to the deepest horizon available. We note that the shallow regolith is almost completely depleted in primary minerals, and enriched in secondary minerals including gibbsite, kaolin (kaolinite and halloysite), Fe (hydr)oxides, and amorphous intermediates such as allophane and ferrihydrite. The deep regolith is less-weathered with some primary minerals remaining, and is marked by the "discontinuities" (i.e., humid, the corestone zone; arid, the carbonate-enriched layer). Particularly, Li abundance (represented by $\tau_{Li,Nb}$, an index of the loss or gain of Li in the regolith, see the Supplementary Information) increased upwards in the shallow regolith and downwards in the deep regolith. We further defined "rhizospheric soils" as part of A horizons (~20 cm depth) with a high density of plant roots. A total of 27 solid samples from the regoliths were collected along vertical profiles, with non-equidistant sampling intervals (i.e., few centimeters to meters). Three Pololu basalts and two Hawi ash samples (~150 ka) (20.043328, −155.734678) were sampled. Plants (humid: fountain grass; arid: buffel grass) and associated water was recovered, such as rainwater, local seawater, groundwater, and river water. All water samples were filtered using 0.22 μm cellulose acetate filters (Whatman™) immediately after sample collection. Then these water samples were acidified using HNO_3 solutions and stored in the cooler at 4 °C.

3. METHODS

3.1. Sample characterization

Regoliths were sampled by horizons from surface soils to pristine substrates, air-dried and crushed. Soil fractions (<2 mm size) were separated by air-dried sieving of the bulk soils. The physicochemical characterizations, including bulk density, soil organic carbon content (C_{org}), and pH were performed at the University of California, Santa Barbara. Soil C_{org} values was measured through dry combustion at 1423 K with an Elementar™ Vario EL III CNS analyzer. Soil pH was measured potentiometrically by a soil–water mix ratio of 1:1 v/v. To obtain refined compositional description of major elements, solids were analyzed by XRF techniques at the ALS Chemex Labs following the $Li_2B_4O_7$ fusion method. Mineralogical analysis was performed on a Rigaku™ XRD diffractometer (Cu/Kα radiation), operating at 40 mA/40 kV. The XRD spectra were obtained in the 2θ range from 20° to 80° at a step interval

of 0.01° and a scan rate of 0.5°•min^{-1} (Fig. S2). Short-range-order (SRO) minerals such as ferrihydrite and allophane were quantified by recording weight loss after NH_4OAC extraction (Chadwick et al., 2003). Major regolith characteristics are tabulated in Table S1.

3.2. Organic matter-Li experiments

To evaluate possible interactions between Li^+ and organic matter, we performed batch experiments by mixing 50 mL humic acid (HA, Aldrich^{TM}) slurry (4 g•L^{-1}) with prepared LiCl solutions (25/250 uM Li) at pH = 4 and 7 in 50 ml polypropylene centrifuge tubes, and equilibrated for 3 days. To avoid artificial isotopic effects from organic matter, HA powders were rinsed with acidic MQ water until Li concentrations were below the detection limit of the instrument. After experiments, an aliquot of filtrate was separately passed by < 0.2 μm and < 0.02 μm filtration (Waterman^{TM}), and < 10 kDa and < 1 kDa (MilliporeTM) ultrafiltration. All size-fractions were determined for both elemental and isotopic compositions of Li.

3.3. Sequential extraction

To understand Li elemental and isotopic behaviors in the shallow regolith, a standardized sequential extraction procedure (Community Bureau of Reference, BCR, Table S2) was used. Lithium distribution among soil compartments was evaluated based on operationally defined extractions of topsoils. It was applied to extract Li hosted in soil fractions including (1) exchangeable fractions (exchangeable and carbonate phases), (2) reducible fractions (Fe/Mn (hydr)-oxides), (3) oxidizable fractions (sulfides and organic matter), and (4) residual fractions (silicate phases). Soil-free blanks were performed, and percent recoveries were calculated from the sum of individual fractions and then compared to the bulk digestion. We noted that Li mass loss occurred during sequential extraction, and only repeats with Li recoveries > 90% were reported (Table S3). To evaluate the mass balance of the BCR protocol, we compared measured δ^7Li values of bulk soils and calculated total soil stocks using the following Eq. (1):

$$\delta^7Li_{Calc} = \sum_{f=1}^{n}(\delta^7Li_i \times C_i^{Li})/\sum_i C_i^{Li} \quad (1)$$

where C_i^{Li} and δ^7Li_i respectively denote the relative Li fraction (a sum of 100%) and the isotope signature of individual fraction obtained from sequential extraction step i (i = 1–4).

3.4. Sample dissolution for elemental analysis

A total of 27 regolith samples (~100 mg) were placed in Teflon beakers and digested via the HF-HNO_3-HCl protocol (W.-Li et al., 2019). In addition, powdered grass samples (freeze-dried) were dissolved in concentrated HNO_3-H_2O_2-HCl mixtures, and heated to > 150 °C for 14 days. Residues were refluxed by concentrated HCl solutions, dried, and then dissolved in 2% HNO_3. Elemental concentrations of sampled material were measured on a Quadrupole-inductively coupled plasma-mass spectrometry (Agilent^{TM} 7900 Q-ICP-MS) at the plasma mass spectroscopy laboratory, University of North Carolina at Chapel Hill. Elemental concentrations were determined using a series of calibration standards of known concentrations. Internal standards, including Be, Ge, Ph, In, Ir, and Bi in 2 % HNO_3, were used to correct instrumental drifts. The analytical errors of concentration analysis are < 2% (RSD).

3.5. Sr isotope analysis

After digestion, Sr fraction was separated following a standard ion exchange protocol (2.5 N HCl, Bio-Rad^{TM} AG50W-X12), and isotopic compositions were measured using a Neptune^{TM} Plus Multi-collector ICP-MS (MC-ICP-MS) at the State Key Laboratory of Marine Geology in Tongji University. During the period of data acquisition, the mass fractionation and the instrument bias were normalized by $^{86}Sr/^{88}Sr = 0.1194$ following the exponential law. $^{88}Sr/^{86}Sr = 0.1194$ was used to calibrate mass bias during isotope analysis, and the NBS SRM 987 standard was measured with samples to confirm the quality of analysis, yielding an average $^{87}Sr/^{86}Sr$ of 0.710271 $\pm 18 \times 10^{-6}$ (2SD, N = 10). Two United States Geological Survey (USGS) basalt standards were adopted for accuracy evaluation, BCR-2 (Columbia River basalt, 0.704995 $\pm 18 \times 10^{-6}$) and BHVO-2 (Hawaiian basalt, 0.703454 $\pm 13 \times 10^{-6}$). Analyses of the two references are consistent with published data (the mean values, 0.704958, BCR-2; 0.703435, BHVO-2) (Raczek et al., 2001; H.-Liu et al., 2012).

3.6. Li chromatographic purification

Lithium fractions in samples were isolated following a dual-column chromatographic method (W.-Li et al., 2019). Before column chemistry, solid samples were digested in a 3:1 mixture of double-distilled HF and HNO_3 at 180 °C on a hot plate until samples were totally dissolved. Samples in aqueous phases were dried, refluxed in aqua regia, and then in concentrated HCl solutions, and subsequently dissolved in 0.2 mol•L^{-1} HCl for further purification. The chromatography was composed of two steps to ensure high sample loading and a fixed elution range. The isolation of Li from most matrices was achieved by cation-exchange chromatography with pre-cleaned Bio-Rad^{TM} AG50W-X8 resin (200–400 mesh), and 0.2 mol•L^{-1} HCl solution as the eluent. The further isolation of Li was achieved using the same resin and 0.5 mol•L^{-1} HCl solution as the eluent. All final solutions after column separation were checked on an Agilent^{TM} 7900 Q-ICP-MS to guarantee high yields (~100%) and low matrix influence (Na/Li < 1) in collections, ensuring the reliability of isotope analysis.

3.7. Li isotope analysis by Q-ICP-MS

The Li isotope analysis was performed using the same Q-ICP-MS instrument as the elemental analyses, and the detail was previously reported in Liu and Li (2019). A brief

description of the analytical method is given here. Prior to isotope analysis, samples and geostandards were matrix matched to a concentration of 0.5 ppb Li in 2% HNO_3. We used an Agilent™ microflow self-aspirating (200 μL•min^{-1}) PFA nebulizer, quartz spray chamber, quartz torch, and 2.5 mm internal diameter injector. To achieve high signal stability and low background, we optimized the carrier gas flow (0.95 L•min^{-1}) and the make-up gas flow (0.35 L•min^{-1}). The instrumental sensitivity was ~250,000 cps on ^{7}Li for 0.5 μg•L^{-1} solution. Because of the low sample size (0.5 ppb), long washing time (180 s) was adopted to maintain low background, so that memory effects can be controlled. For each sample, the ratio of concentration of all matrix elements to lithium is limited to be < 2 to eliminate potential matrix effects. The sample-standard bracketing method was employed, and the concentration match between samples and standards was limited to be > 95%. We reported Li isotopic composition expressed as $\delta^{7}Li=\{[(^{7}Li/^{6}Li)_{sample}/(^{7}Li/^{6}Li)_{standard}]-1\}\times 1000$, relative to the IRMM-016Li standard. The long-term external precision is 1.1‰, from the 2SD of nearly one-year repeat analyses of IRMM-016 and USGS igneous rock standards JG-2 and BCR-2 (Liu and Li, 2019). During the course of this study, we used two USGS basalt standards BCR-2 and BHVO-2 to ensure accuracy for Li isotopic analysis. The BCR-2 yields δ^{7}Li of 2.92‰ (N = 10), and the BHVO-2 yields δ^{7}Li of 4.74‰ (N = 10) with a long-term 2SD of ± 1.1‰ (Table S4), falling within the isotope range reported in previous studies.

4. RESULTS

4.1. Li mobilization and distribution

Chemical depletion profiles of specific elements are shown in Fig. 2, and listed in Table S5. Element mass transfer function (τ) calculation is given here (Chadwick et al., 1999), and the detailed expression is given in the supplementary information (SI):

$$\tau_{x,w}=\rho_{w}C_{x,w}\rho_{p}C_{x,p}(\varepsilon_{x,w}+1)-1) \quad (2)$$

where $\varepsilon_{x,w}$ is the strain factor (an index of soil volume change), $C_{x,p}$ is the concentration of element x in the protolith (e.g., unweathered parent material, bedrock), $C_{x,w}$ denotes the concentration of element x in the weathered product, and ρ_p and ρ_w are the bulk density of the protolith and weathered soils, respectively.

Here, we divided the regolith profile into two parts (see explanation in the Section 2.2) regarding the extent of Li depletion: (i) less-depleted or enriched shallow regolith (Fig. S3); (ii) partially depleted deep regolith. The Li concentrations increased upward to an order of magnitude higher, from 7,170 ng•g^{-1} to 65,410 ng•g^{-1} (humid) and 32,440 ng•g^{-1} (arid), respectively. Similar patterns have also been found in an arid site E (MAP = 570 mm) and a humid site J (MAP = 1,380 mm) along the Hawi lava climosequence (Huh et al., 2004). The Li stocks in the plant samples (70 ~ 350 ng•g^{-1}) were much lower than bulk soils, consistent with reports of low Li bioavailability (e.g., Lemarchand et al., 2010; Pogge von Strandmann et al., 2012; Clergue et al., 2015). Elemental ratios for Li/Nb and Li/Na Indicate Li enrichment in both strongly and weakly weathered regoliths. The elemental ratios increased upward to the maximum in the shallow regolith (<1m), and gradually approached to the Li/Nb and Li/Na ratios of the vegetation grown on the top.

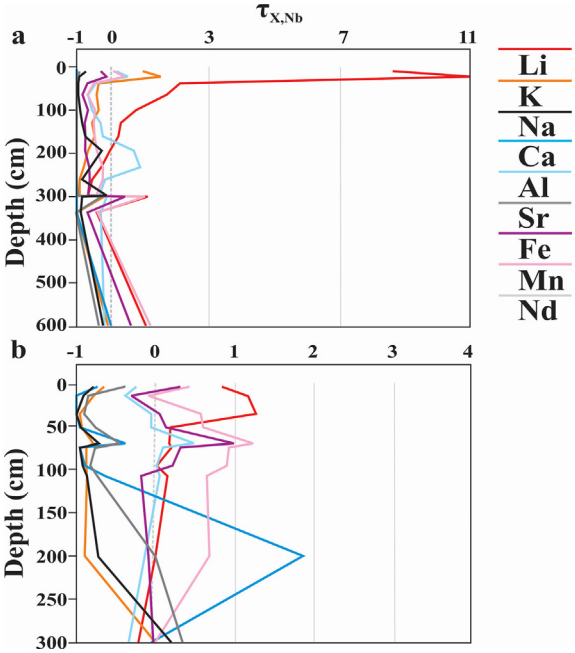

Fig. 2. In-depth cation mass transport functions of (a) the humid (BE) regolith, and (b) the arid (PO) regolith.

The shallow regolith exhibits local-scale enrichment of Li and some rock-derived elements (e.g., K, Mn, Fe, and Al) in the surface soils (Fig. 2), reaching the maximum $\tau_{Li,Nb}$ of 10.9 in the humid site and $\tau_{Li,Nb}$ of 2.8 in the arid site. Different from observations made by Huh et al. (2004), the organic-rich soil layers (O horizons and upper A horizons) display high Li contents (up to 60 ug/g). Calculated Li mass flux in a vertical order ranges from −0.01 to 0.55 mg•cm^{-2} (humid) and −0.02 to 1.78 mg•cm^{-2} (arid), exhibiting similar patterns as $\tau_{Li,Nb}$, reaching the maximum in rhizospheric soils (Figs. 2 and 3). As a result of absolute accumulation, integrated net Li mass gains in the shallow regolith are 30.6 mg•cm^{-2} (humid) and 40.6 mg•cm^{-2} (arid), respectively. The average rates of Li mass gain were calculated to be 0.09 μg•yr^{-1}•cm^{-2} (humid) and 0.12 μg•yr^{-1}•cm^{-2} (arid), respectively, based on an assigned age of 350 ka for the Pololu lava. Although Li^{+} is more prone to be leached from regoliths than high field strength elements (e.g., Zr, Nb, Ta, Ti and Th, Liu et al., 2013), preferential retention of Li with respect to Nb is found in both humid and arid shallow regoliths.

4.2. Bulk isotopic compositions

The basalt substrates display an average δ^{7}Li of 2.2‰, within analytical error (±1.1‰) of that reported for Hawaii basalts (Mauna Loa flows, δ^{7}Li of 2.8–3.1‰, Pistiner and

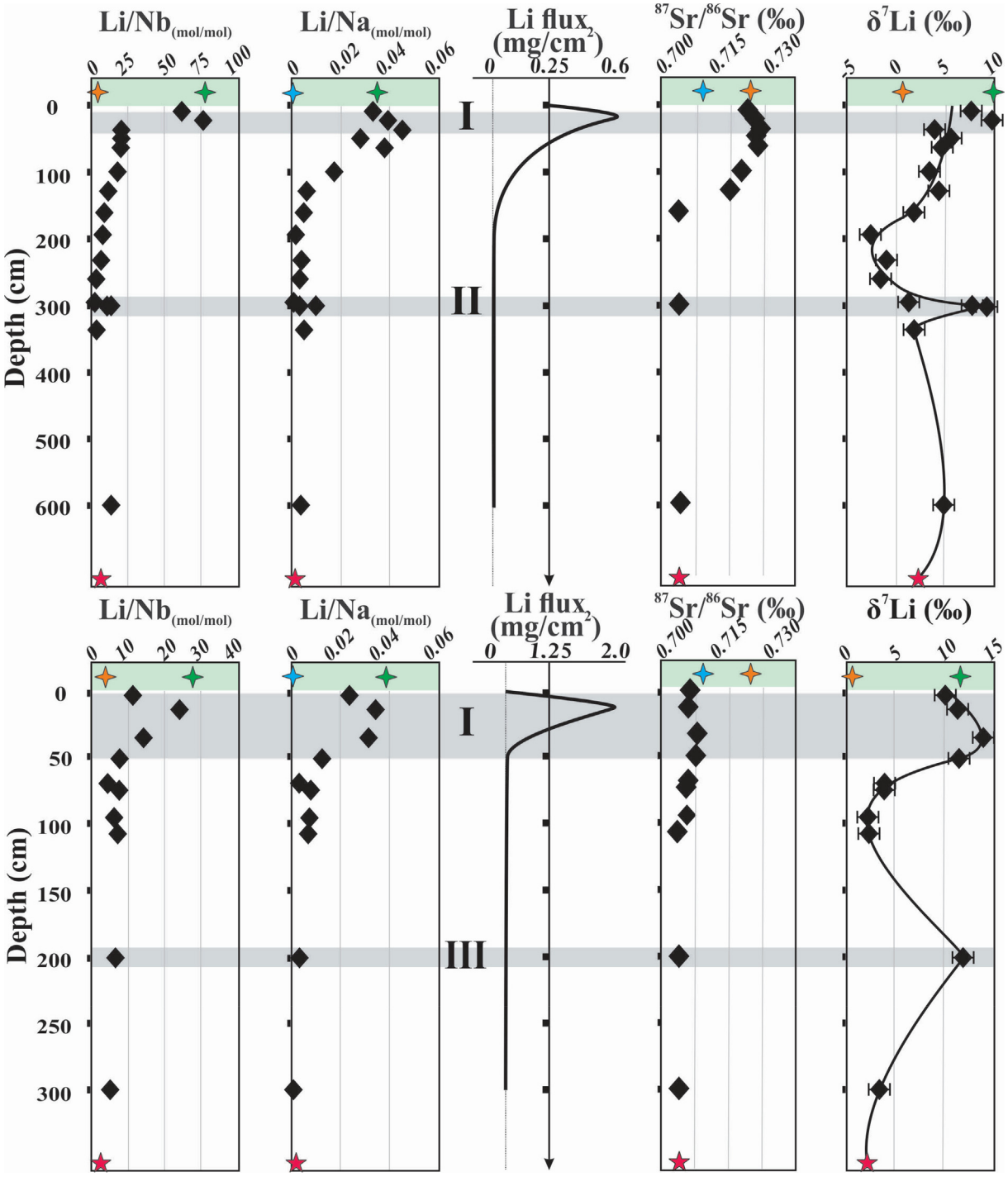

Fig. 3. In-depth characterization of the humid (BE, upper panel) and the arid (PO, lower panel) regolith profiles, including Li/Nb and Li/Na molar ratios, Li mass flux, $^{87}Sr/^{86}Sr$ and δ^7Li signals. The grey region I indicates the surface horizon with remarkable Li gains; the grey regions II and III denote the "regolith discontinuities": the corestone zone in the humid regolith and the carbonated-enriched layer in the arid regolith, respectively. The blue stars represent marine aerosol (seawater, $^{87}Sr/^{86}Sr = 0.7092$, Hess et al., 1986). The green stars indicate collected bulk grass. The yellow stars represent dust deposition (continental dust, $^{87}Sr/^{86}Sr \sim 0.722$, Lam et al., 2013; the upper continental crust, $\delta^7Li = 0.6‰$, Sauzéat et al., 2015). The red stars at the bottom represent the composition of parent Pololu basalt.

Henderson, 2003) (Table S5, Fig. 3). The shallow regolith (<1m) displays a wide range of heavier Li isotopic compositions than that of the parent basalt. The δ^7Li values of weathering residues range from −2.7‰ to 9.9‰ in the humid site, and from 2.2‰ to 13.9‰ in the arid site. Samples with lighter isotopic composition than basalt in the

upper section of the deep humid regolith can be explained by the preferential scavenges of the light Li by clays (Pistiner and Henderson, 2003). In the humid regolith, δ^7Li gradually reaches a heavy composition of 9.1‰ near the discontinuity divided by the corestone zone (Region II, Fig. 3), and decreases upwards to −2.7‰ at ~2 m depth in the deep regolith. In the shallow regolith, δ^7Li increases towards soils that reach an isotopic plateau of ~4.0‰, then sharply raises up to 9.9‰ near the top of the regolith. In the arid regolith, δ^7Li increases from 3.3‰ to 11.8‰ at the carbonate-enriched layer (Region II, Fig. 3), and decreases upwards to ~2.2‰ at 1 m. The δ^7Li values of the shallow regolith are heavy, showing a positive excursion in soils with a peak value of 13.9‰, and ultimately decrease to 10.1‰ in the topsoil. Bulk plants (Table S5) from humid/arid sites share nearly identical Li isotope compositions around 9-10‰, while the Li isotopic compositions in plant tissues vary. The δ^7Li values of roots/rhizomes (12.2–13.6‰) are higher than the δ^7Li of rhizospheric soils (<20 cm, 9.9–11.3‰). Grass roots/rhizomes are isotopically heavier than stems by up to 3.4‰. Stems are isotopically heavier than the grass-foliage ($\Delta^7Li_{stem\text{-}foliage}$ up to 2.9‰). The δ^7Li value of river water at the humid side is 15.4‰, very close to that of sampled groundwater (11.1–18.3‰), and that of exchangeable soil fractions by the BCR extraction (10.3–16.4‰). The rainfall sample has a δ^7Li of 25.1‰, lower than that of the marine aerosol (30.5‰). The $^{87}Sr/^{86}Sr$ signals in the arid regolith are mostly homogeneous (0.703309–0.706129), approaching to a basalt-like feature (0.703774), and the humid shallow regolith has much more radiogenic $^{87}Sr/^{86}Sr$ (0.718142–0.722325) compared with that of the deep regolith (0.703958–0.715493).

4.3. Li distribution and isotopic ratios in soil fractions

The Li concentration and δ^7Li in the sequential-extracted fraction of soils from the shallow regolith are tabulated in Table S3, and displayed in Fig. 4. As expressed relative to the bulk soil mass, Li yields range from 98% to 102%. Notably, soil Li was heterogeneously distributed in fractions, showing Li mobilization and redistribution in compartmentalized soil fractions. The residual fractions preferentially scavenged light ^{6}Li, showing a range of 86–93% total Li in the humid regolith and a range of 59–84% total Li in the arid regolith. Because only a trace amount of Li resides in quartz, its influence on residual (silicate) fractions should be negligible. The exchangeable soil fractions demonstrate the lowest Li content, accounting for < 2% Li. The reducible fraction is the second-largest reservoir, particularly in the arid regolith (3–28%). Soil oxidizable fractions have a small Li fraction of 1–5%, and no statistically significant correlation between soil Li content and soil organic carbon (C_{org}) can be found.

Following the BCR sequential extraction, Li fractions in four extractions spanned a wide range of isotopic compositions compared with bulk soil compositions (Fig. 4). The match between measured and calculated soil δ^7Li verifies the applicability of the sequential extraction within analytical uncertainties (Fig. S4), which is expected because of the complete recoveries of extracted Li fractions. Previous stud-

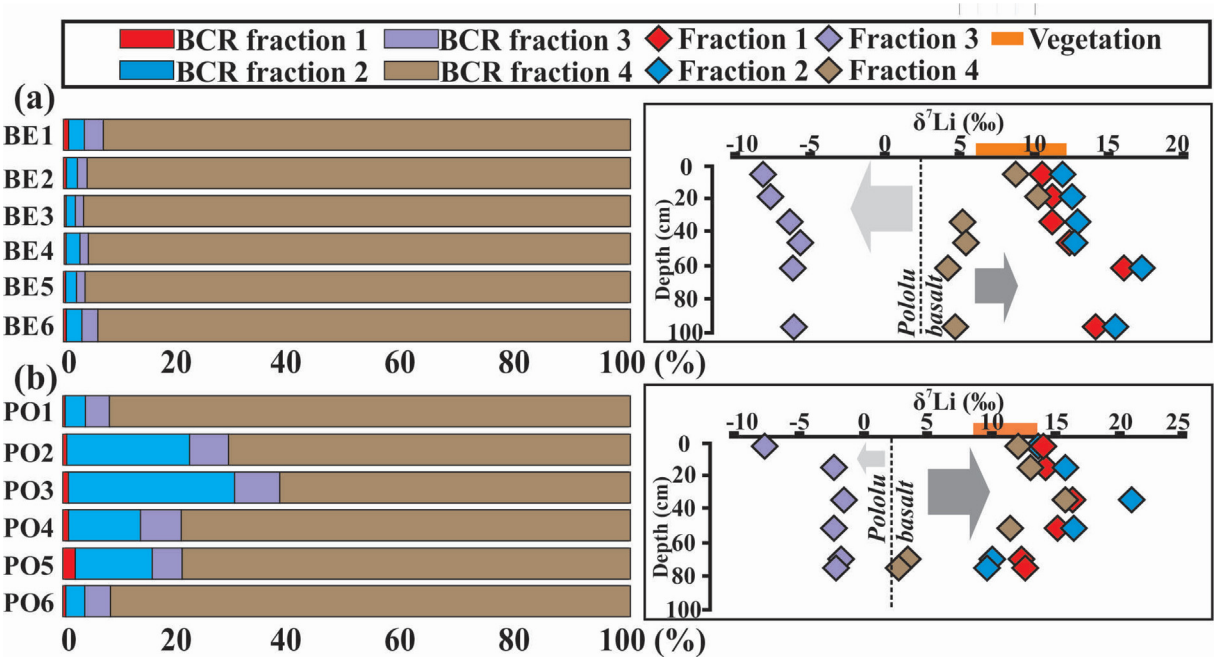

Fig. 4. In-depth variations of the relative proportions of Li in soil extractions relative to the bulk (left panel) and the δ^7Li ratio of soil fraction (right panel) in (a) the humid regolith and (b) the arid regolith. Fraction 1 represents exchangeable components and carbonates; fraction 2 represents the Fe and Mn (hydr)-oxides; fraction 3 represents organic phases; and fraction 4 represents residual silicates. Error bars on the x-axis refer to the long-time reproducibility (2SD = 1.1‰) of Q-ICP-MS analysis, which is smaller than the symbol sizes.

ies have shown that soil residual fractions presumably made up of clay minerals are isotopically lighter than their parent basalt (e.g., Vigier et al., 2008; Hindshaw et al., 2019; Pogge von Strandmann et al., 2019; Li and Liu, 2020). However, we found that Li trapped in residual soil fractions is isotopically heavy (humid, 4.2–10.1‰; arid, 2.8–15.8‰), compared to their parent rock (2.2‰). The residual fractions of topsoils are heavier than that of subsoils by up to ~7‰ in the humid site. Soil exchangeable (10.3–16.4‰) and reducible (11.1–17.2‰) fractions are isotopically similar. Mean δ^7Li differences between soil exchangeable/reducible fractions and soil residual fractions are 8.4‰ (humid, BE) and 4.1‰ (arid, PO), respectively. Substantial enrichment of light Li was found in soil oxidizable fractions, ranging from −8.2‰ to −5.7‰ (humid, BE), and from −7.7‰ to −1.5‰ (arid, PO), respectively.

4.4. Li distribution and isotopic ratios in humic fractions

Since plants and soil organic fractions are rich in light Li isotopes, long-term biological influences on terrestrial Li isotope fractionation require investigations. To examine the influence of soil organic matter on Li isotope behavior, we experimentally tested the fractionation of Li isotopes by organic molecules of different sizes. Lithium partitioning and isotope fractionation in experimental HA-Li interactions using filtration and ultrafiltration methods are illustrated in Fig. S5. In a low Li loading setting (25 μM), about 13% total Li remained in the 1 kDa-0.2 μm fractions at pH = 4, while ~21% total Li was recovered in the 1 kDa-0.2 μm fractions at pH = 7. Compared with the initial LiCl source (δ^7Li = 5.8‰), dissolved δ^7Li in filtrates ranges from 4.4‰ in the < 0.02 μm fractions to 5.3‰ in the < 1 kDa fractions at pH = 4, and from 3.3‰ in the < 0.02 μm fractions to 5.0‰ in the < 1 kDa fractions at pH = 7, respectively. The δ^7Li values in different size-fractions at pH = 4 are identical, within the analytical uncertainty (2SD = 1.1‰), to that of the initial Li solution (δ^7Li of 5.8‰). The outcome confirms apparent Li isotope fractionations between Li pools at pH = 7. The retention of isotopically light Li in the 10 kDa-0.02 μm fraction reveals that medium-weighted organic molecules rich in functional groups (e.g., aromatic moieties) preferentially complex with the light Li. In the high Li loading setting (250 μM), almost all Li resides in the < 1 kDa fractions, regardless of pH change. The δ^7Li values in all size-fractions are similar to the initial Li source (LiCl, 5.8‰). There is no distinguishable isotope fractionation among size-fractions with high Li/TOC ratios.

5. DISCUSSION

5.1. Atmospheric addition

5.1.1. Evidence from soil chemistry

Observed Li enrichment in soils suggests the atmospheric deposition derived from two main sources (Fig. 2). The addition of tephra from more recent Hawi eruptions (~150 ka) could have contributed Li to the surface of the soils, because Li concentration in Hawi volcanic ejecta is ~9.5 ug/g slightly higher than that of the Pololu basalt (~6.5 ug/g). Furthermore, the high Li concentration in long-distance transported continent dust (i.e., the Li chemistry of dust is taken as equal to that of the upper continental crust, 30.5 ± 3.6 ug/g Li, Sauzéat et al., 2015) probably results in the near-surface Li enrichment (Table S5). Accreted volcanic ash could affect Li abundance in soils, but may not alter δ^7Li relative to that of underlying basalt, due to their similar chemical and isotopic compositions. To simplify the calculation, ash fractions are not distinguished from primary basalt fractions. Since studied Hawaii soils develop over time, atmospheric addition exerts cumulative impacts on the geochemical budget of the shallow regolith, providing additional Li and crustal Li isotopic signatures. Likewise, the Li accumulation and heavy δ^7Li in Hawaiian soils were explained by eolian and marine aerosol additions along with climatic and chronologic changes (Huh et al., 2004; Ryu et al., 2014).

5.1.2. Evidence from soil Li-Sr isotope mixing

The "bowed" shape of Li isotopic compositions in the shallow regolith is probably produced by the addition of dissolved or particulate Li from dust or seawater (Fig. 3). Soil Li abundance positively correlates with soil δ^7Li values (Fig. 5). The δ^7Li of upper soils converges to ~10.0‰, revealing external Li components of heavy isotopic signatures. Based on the slope of the linear fitting, the arid regolith preserves more marine-derived Li signals than the humid regolith. Here, we consider that seawater imprints on soils introduced by sea salt-enriched liquid droplets or evaporated particulates could be preserved during strong evapotranspiration in the arid site (Hsieh et al., 1998). The preservation of seawater signals is also true for Sr and its radiogenic isotopes at the South point of the Island of Hawaii, under a semi-arid climate (Whipkey et al., 2000). The lighter δ^7Li signal of rainwater than seawater δ^7Li can be attributed to dissolved dust components (δ^7Li = 0.6 ± 0.6‰, the upper continental crust, Sauzéat et al., 2015) that dilutes the marine signals. Not surprisingly, global rainfall compilations display large Li isotopic variations in both oceanic settings (e.g., 33.3‰, snow, Iceland, Pogge von Strandmann et al., 2006; 33‰, Azores Archipelago, Pogge von Strandmann et al., 2010; 11.2–26.4‰, throughfall, Guadeloupe, Clergue et al., 2015) and continental settings (3.2–95.6‰, monitoring stations in Brest, Dax, Orléans, Thonon and Avignon, France, Millot et al., 2010a; 26‰, the Mackenzie Basin, Canada, Millot et al., 2010b; 9.3‰, Yellow River, Gou et al., 2019), implying strong local and seasonal dependence.

The data of quartz-enriched surface horizons in the humid regolith provide quantitative evidence of dust addition (Fig. S2). The correlation between quartz contents and δ^7Li signals in the shallow regolith of the humid profile indicates that dust addition exerts a vital control on Li isotopic variations in the humid regolith (Fig. 6). The most radiogenic Sr isotope signal occurs in the humid shallow regolith, highlighting the influence of slow but continuous eolian dust addition ($^{87}Sr/^{86}Sr \sim 0.722$, Lam et al., 2013). Therefore, the eolian addition gradually replaces the original basalt Sr that has been depleted by chemical leaching.

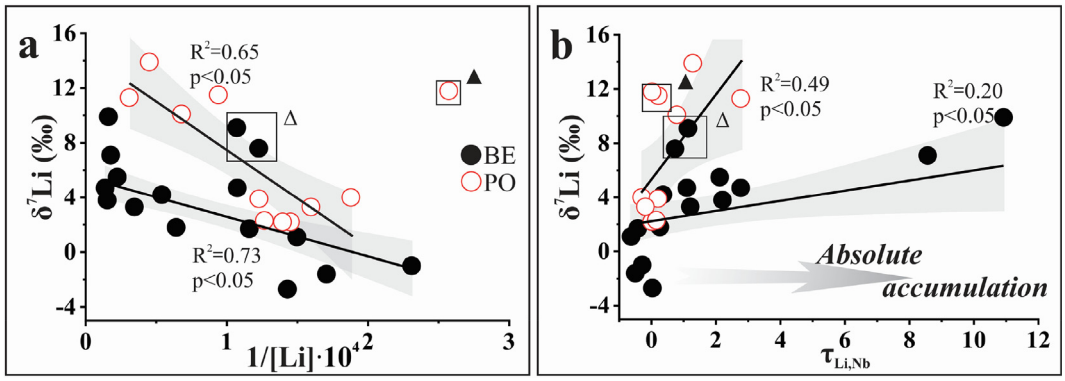

Fig. 5. Li isotope fractionation as a function of (a) 1/[Li] and (b) $\tau_{Li,Nb}$. Linear smoothers are shown with black lines, and the shaded areas represent the 95% confidence intervals. Data points located in boxes were excluded for linear fitting due to anomalous δ^7Li. In the plot, Δ denotes the corestone zone in the humid regolith, and ▲ denotes the carbonate-enriched layer in the arid regolith.

The arid shallow regolith exhibits mixed $^{87}Sr/^{86}Sr$ values derived from both basalt (0.7038) and marine aerosol (0.7092). The deep regolith is barely influenced by atmospheric deposition, evidenced by its homogeneous $^{87}Sr/^{86}Sr$ (0.703–0.704, equal to the basalt signals). We assume that leaching only has limited influence on soil Li in the shallow regolith, since the Li isotopic values of the shallow regolith are heavier or equal to basalt isotopic compositions. Herein, we infer that the soil Li-Sr isotope signals reflect a mixing of three dominant end-members, following Eqs. (3), (4) and (5):

$$f_P + f_D + f_S = 1 \quad (3)$$

$$f_P C_P \delta^7 Li_P + f_P C_P Li_D + f_S C_S \delta^7 Li_S = (f_P C_P + f_P C_P + f_S C_S) \times \delta^7 Li_{Soil} \quad (4)$$

$$f_P c_P \delta^{87}Sr/\delta^{86}Sr_P + f_D c_D \delta^{87}Sr/\delta^{86}Sr_D + c_S f_S \delta^{87}Sr/\delta^{86}Sr_S = (f_P c_P + f_P c_P + f_S c_S) \times \delta^{87}Sr/\delta^{86}Sr_{Soil} \quad (5)$$

where (f_P, f_D, f_S), (δ^7Li_P, δ^7Li_D, δ^7Li_S) and ($^{87}Sr/^{86}Sr_P$, $^{87}Sr/^{86}Sr_D$, $^{87}Sr/^{86}Sr_S$) represent the fractional contributions of Li isotopes and radiogenic Sr isotopes from parent basalt (P), dust (D) and seawater (S), respectively. The C and c denote the concentrations of Li and Sr in each com-

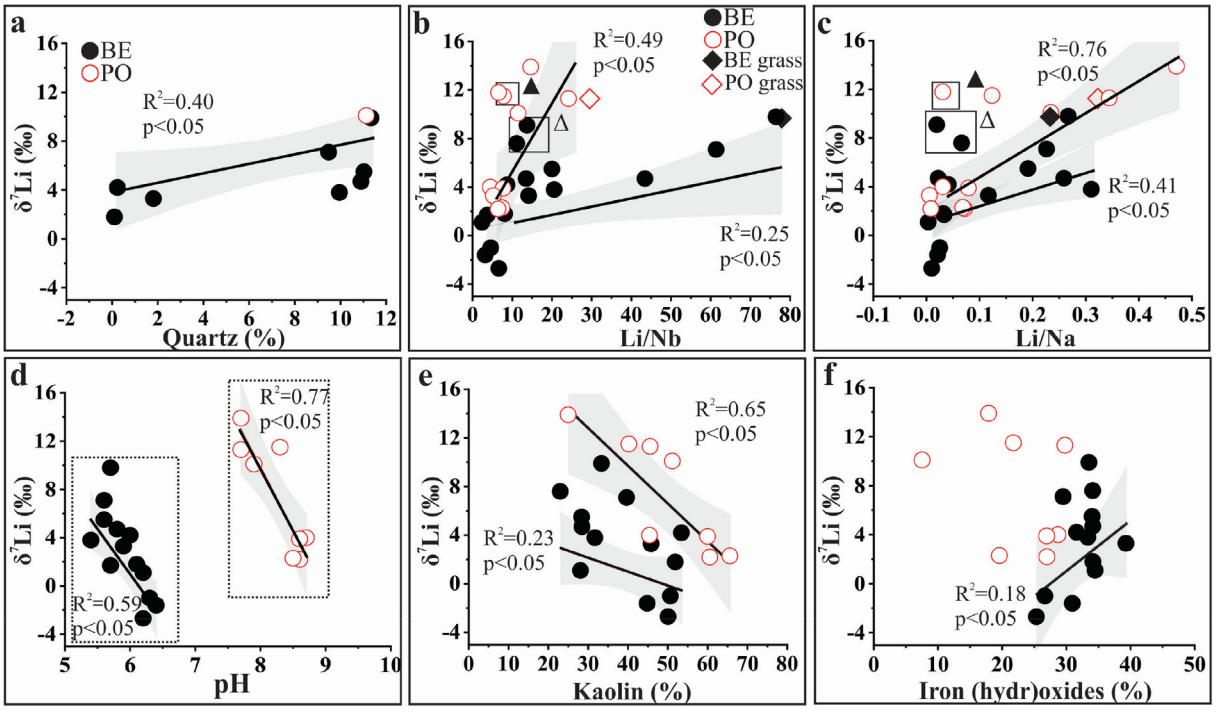

Fig. 6. Regolith Li isotope fractionation as a function of (a) quartz contents, (b) Li/Nb ratios, (c) Li/Na ratios, (d) regolith pH, (e) kaolin group abundance, and (f) Fe (hydr)-oxide contents. Linear fittings are shown by black lines, and the shaded areas reveal the 95% confidence intervals. Data points in the boxes were excluded for linear fitting. Δ: The corestone zone in the humid site; ▲: The carbonate-enriched layer in the arid site.

partment, respectively. On the δ^7Li versus $^{87}Sr/^{86}Sr$ diagram (Fig. 7), the isotope composition of each end-member and uncertainties theoretically define the multi-component mixing envelopes. We observe that dust addition is significant in the humid regolith, while the isotope contribution of seawater can be identified in the arid regolith despite low rainfall. Porder et al. (2007) also demonstrated a strong rainfall dependence on the dust addition to Kohala soils. We note that this mixing plot only provides a lower limit of marine contribution, since light Li prefers to be scavenged into clays (Vigier et al., 2008).

5.1.3. Evidence from pore water extraction

Soil pore water extraction provides additional insights into the atmospheric contribution. The Li addition from wet and dry deposition (containing marine aerosols) is mostly preserved in the soil solutions extracted from the shallow regolith. In both arid and humid regoliths, heavier Li isotopic compositions in soil residual fractions (Δ^7Li up to 10.9‰) in the shallow regolith reflect the deposition from isotopically heavy Li of seawater origin. In Kohala soils, neo-formed secondary minerals preserve the oxygen isotopic signal of the soil solution (Ziegler et al., 2003). Thus, we suggest that it may be applicable for soil Li isotopes as well. Local water balance (i.e., rainwater infiltration vs. evapotranspiration) is closely related to the migration of pore water, and the water-balance threshold of MAP $\sim$ 500 mm·a^{-1} for Hawaiian soils was reported (Hsieh et al., 1998). Using soil oxygen isotopes, Hsieh et al. (1998) quantified evapotranspiration relative to precipitation along the Kohala climosequence. The arid regolith loses water by evapotranspiration with Li enrichment in secondary products, and a part of soil Li was derived from the marine aerosol. Nearly all rain into those areas is evaporated from arid soils (and plants on top). Therefore, marine signals could be retained in arid soils, despite limited rainfall. In the humid regolith, isotopically heavy Li dissolved in the seepage can be easily transported into the deep regolith and/or nearby runoff, because of the positive water balance (precipitation > evapotranspiration). Next, dust-derived isotopically heavy Li signals can be partially inherited in the shallow regolith through soil formation in the humid regolith. In addition, the preservation of marine signals may be ascribed to long-neglected biological cycle as well, which is discussed in details in the next Section 5.2.

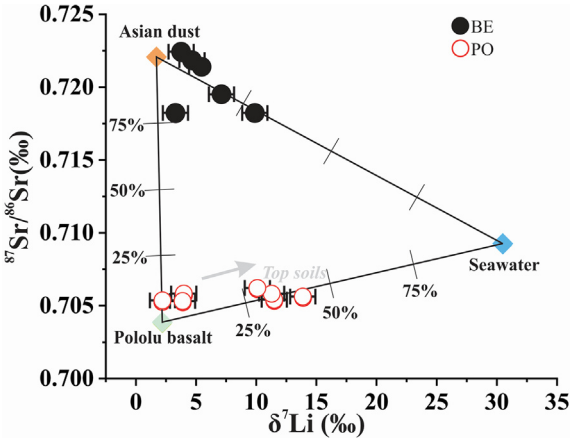

Fig. 7. δ^7Li versus $^{87}Sr/^{86}Sr$ of the shallow regolith in the humid and arid sites. Solid lines denote a theoretical isotope mixture in molar fractions between end-member values.

5.2. Vegetation cycling

Phytoextraction and subsequent deposition in necromass induce substantial elemental distribution in soils; we use the term bio-lifting to describe this process. The function of Li in plant physiology has been emphasized in the literature (e.g., Anderson, 1990; Shahzad et al., 2016, and references therein). For example, Robinson et al. (2018) suggested that soluble Li in soils can be taken up into leaves without a reduction in plant biomass in New Zealand, producing a bioaccumulation coefficient larger than 5. Kalinowska et al. (2013) used hydroponic experiments and demonstrated that lettuce accumulated Li in leaves at concentrations tenfold higher than the original nutrient solutions. Thus, we consider that biological influence on soil Li could not be excluded. Rather, several lines of evidence support the importance of biological effects on natural Li cycling between soils and plants and within plant organs and tissues in the studied area.

5.2.1. Evidence from soil-plant Li isotopes

The δ^7Li values in plant tissues vary from 6.2 to 13.6‰ with a mean value of 9.8‰. Plant δ^7Li values are lighter than the Li isotopic compositions of the exchangeable and reducible soil fractions that range from 11.2 to 21.0‰ with an average of 13.8‰. It is shown that the isotopic composition of temporal pore water could be reflected by soil exchangeable and reducible fractions (e.g., Wiegand et al., 2005; White et al., 2009; Bullen and Chadwick, 2016). Intra-plant transport probably allows the upward transfer of light Li isotopes, since light Li isotopic compositions have been found in leaves (Table S5). Litterfall returns isotopically light Li into soils annually, which results in isotopically light Li in soil oxidizable fractions (Table S3). From the result of the sequential extraction, estimated δ^7Li values in pore water (i.e., soil exchangeable fractions) are 13–14‰, lower than rainwater δ^7Li (14.3–25.1‰). Therefore, we interpret the Li signal of pore water as a weighted sum of: (i) marine-derived Li, (ii) basaltic Li from the parent rock and dust during dissolution, (iii) residual Li in pore water, and (iv) Li from litterfall. It is supported by isotopically light Li in soil exchangeable and reducible fractions, and increases in the isotopic heaviness of soil bioavailable fractions with depth (Fig. 4). Bio-cycled Li is released into soil at or near the surface, whereas rock Li is released by weathering throughout the soil but particularly near the regolith – rock contact and therefore rock Li is more likely to be leached. It is a continuous process which can feed differences in Li isotopic signals that is incorporated into secondary minerals at different depth locations.

5.2.2. Evidence from intra-plant Li isotopes

Differential δ^7Li signals in higher plants have been reported so far ($\Delta^7Li_{max} > 16‰$, spruce and beech, Myška et al., 2010; 3.1‰, spruce, Lemarchand et al., 2010; 1.3‰, spruce, Clergue et al., 2015). In this study, grass foliage bears lighter δ^7Li (6.2–8.7‰) than stems (9.1–10.2‰) and roots (12.2–13.6‰), revealing upward ^{6}Li transport in plants. Such a feature may be attributed to ion diffusion via a chromatographic-like process (Bagard et al., 2013). The isotope fractionation of Li among the stems, branches and leaves might result from chromatographic exchange, enriching ^{6}Li in carboxylate (RCOO-) sites (Putra et al., 2018). In contrast, Myška et al. (2010) reported isotopically heavier Li in stems than roots for *Picea sp.* and *Fagus sp.* Specific isotope fractionation among plant types (angiosperm or gymnosperm) prevailing in (sub)tropical regions have not been systematically studied, and can be vastly different in magnitudes as mentioned for Mg isotope studies (Opfergelt et al., 2014; Chapela Lara et al., 2017; Kimmig et al., 2018). The physiological properties of Li (i.e., availability and bio-sensitivity) have been studied (Anderson, 1990; Gillaspy et al., 1995; Barker and Pilbeam, 2016; Robinson et al., 2018). Therefore, it is reasonable to expect Li partitioning and isotope fractionation in soils relevant to plant growth. Hyperaccumulation and biolifting of soil elements have been addressed in a series of studies (e.g., Bullen and Chadwick, 2016; Gupta et al., 2019; Hausrath et al., 2011; Palumbo et al., 2000; Stille et al., 2009), providing context for interpreting net Li accumulation in soils. Such processes may exert a crucial control on the translocation of nutrients, nonessential (toxic) heavy metals like Cu, Co, Ni, Cr and rare earth elements, and even conservative elements as Zr into the rooting zones.

5.2.3. Evidence from soil Li enrichment

The peak accumulation of Li in the rhizospheric soils has been observed in the humid ($\tau_{Nb,Li} = 10.9$) and arid ($\tau_{Nb,Li} = 2.8$) regoliths. One possible explanation is the apparent dust accumulation in surface soils. The extent of Li enrichment is particularly significant in the humid regolith with dense vegetation coverage. Based on homogeneous $^{87}Sr/^{86}Sr$ signals in soil horizons, vertical distribution of dust fractions within the shallow regolith should be homogeneous. So, the peak Li enrichments found in topsoil horizons cannot be fully explained by atmospheric inputs. Alternatively, it may be a consequence of biologically mediated accumulation. Hence, we postulate that the soil Li enrichments are related to the development of the "biogenic profiles" (Fang et al., 2019). Such a process normally exhibits distinct peak enrichments of elements at or close to regolith surfaces, which is associated with release promoted by organic medias and accumulation in rooting zones (Brantley and White, 2009). If released elements are taken up by plants, or recycled into the rhizospheric soils, and a biogenic profile develops (Jobbágy and Jackson, 2001). Previous studies revealed the importance of vegetation pump in redistributing nutrient as well as non-nutrient metals (Reimann et al., 2009; Imseng et al., 2018). Consistently, the rooting zone has heavy δ^7Li compared with that of adjacent soil layers (Table S5). The ratios of Li/Nb and Li/Na in bulk soils systematically increase upward, and Li isotopic compositions approximate plant signals in surface soils (Fig. 3). We observe overall positive correlations between Li/Nb and Li/Na ratios with δ^7Li values in the regolith ($R^2 = 0.25–0.76$). The element ratios and Li isotope compositions became systematically close to those of bulk vegetation (Fig. 6) rather than dust or ash compositions (Table S5). This feature may be explained by the plant dieback effect or the plant dilution effect (Lemarchand et al., 2010). We consider that biological controls on Li isotopic compositions in rivers and seawater should be negligible since the plant Li fraction is much lower than silicate fractions. However, Li isotopic compositions in aging forest soils could be influenced by biogeochemical processes, as explained in this study.

5.2.4. Evidence from humic size-fraction Li

Sequential extraction experiments suggest that soil organic matters (humic substances) play a role in Li cycling, showing large isotope variations (Fig. 4). Organic matter is expected to promote silicate dissolution and Li desorption from secondary minerals. Thus, organo-mineral associations minimize Li retention and its isotope fractionation, as supported by the low δ^7Li of the organic-rich "black waters" compared to the organic-poor "clear waters" in the Amazon River (Dellinger et al., 2015). Further insights into bio-interferences on isotopic behaviors were gained with the aid of size-fraction analysis of HA-Li association. Despite large errors, we suggest that medium-size humic molecules (1 kDa-0.02 uM) preferentially complex with light ^{6}Li (Fig. S5). The complexation between HA and Li becomes more obvious at pH = 7, corresponding to the dissociation of functional groups (Zhang et al., 2017). The negative δ^7Li associated with organic phases could be explained by the following mechanisms: (i) supply of light Li by litterfall; (ii) complexation of isotopically light Li with humic substances produced from biodegradation; (iii) associations of organic coatings and Li prior-adsorbed on clays.

5.3. Secondary mineral synthesis

In addition to weathering, the patterns of Li are determined by surface adsorption and subsequent incorporation into secondary mineral structures. The Li isotope fractionation could be promoted during the deprotonation of surface hydroxyl groups with increasing pore water pH. Increasing soil pH along depth profiles can facilitate high uptake ratios of Li, driving bulk soils to lighter δ^7Li (Fig. 6). Therefore, pore water with heavier Li isotopic compositions would be transported downwards, and then accumulated in the "regolith discontinuities". This supports the development of high δ^7Li values by pore water infiltration and subsequent deposition. Moreover, mobilized elements could be withheld from rapid leaching by chemically reactive colloids, acting as capillary barriers impeding eluviation. Still, these potential sinks for Li are relatively minor since the Li abundance in soil exchangeable fraction is small, compared to soil residual fractions. It seems likely that Li adsorption on clay surfaces leads to subsequent clay incorporation (Huh et al., 2004) with

consequent preservation of heavy Li signals. Despite strong leaching loss in the humid site, it seems that Li is scavenged by secondary silicates, when combined with bio-lifting, leads to Li peak accumulation in the rhizospheric soils. Clays and soils/saprolites demonstrate large variations in δ^7Li, ranging from −20.2‰ to 26.8‰, relative to the Bulk Silicate Earth (BSE, ~4‰, Penniston-Dorland et al., 2017). Both laboratory experiments and natural observations reveal that Li isotope fractionation during weathering is mineral-specific (Clergue et al., 2015; Millot and Girard, 2007; Pistiner and Henderson, 2003; Pogge von Strandmann and Henderson, 2015; Wang et al., 2015; L. Zhang et al., 1998). The sequestration of Li in secondary aluminosilicates (e.g., kaolinite) have been regarded as one of the dominant isotope fractionation mechanisms for weathering residues. Soil Li isotope compositions correlate with kaolin abundance not Fe (hydr)oxides (Fig. 6), indicating adsorption on kaolinite rather than Fe (hydr)oxides probably drives ^{6}Li retention in soils.

In contrast, atmospheric and biological processes exert little influence on the deep regolith, whereas water percolation and ion accumulation control the fate of Li. The narrow range of $\tau_{Li,Nb,}$ shifts from intermediate loss to gain (Fig. 2). So, the deep regolith could be further divided into two separate parts, (i.e., "depletion-enrichment profiles", Fang et al., 2019), divided by the "regolith discontinuities" including the corestone zone in the humid profile and the carbonate-enriched layer in the arid profile. The regolith above the "discontinuities" showed light δ^7Li values and moderate Li loss upwards, in a large part promoted by the preferential retention of ^{6}Li over ^{7}Li in the regolith during clay formation. Lithium gains or losses were not apparent in the arid regolith, because of restricted Li mobilization within the stagnant fluid-pore networks. At the "discontinuities", heavy δ^7Li exist in both sites while net Li gains only present ($\tau_{Li,Nb} = 1.13$) in the humid regolith. Rapid weathering of the lava provides available Li that dominates vertical migration. To account for the Li anomalies at the "discontinuities", several possibilities are proposed here: (i) preferential retention of original Li stock during weak alteration of the corestones; (ii) extra derivations from neighboring weathered detritus by downward-percolating meteoric waters enriched in isotopically heavy Li passing through the deep regolith; (iii) seasonal infiltrative pulses with atmospheric signals led to heavy δ^7Li during carbonate precipitation; (iv) downward transfer of pore water with heavy Li signals driven by clay formation. The regolith horizon below the "discontinuities" shows upgradient heavier δ^7Li signature, potentially derived from the down-seepage enriched in ^{7}Li, and subsequent concentration at deeper levels of the regolith. This is supported by the relative enrichment of most cations compared with the feature of the shallow regolith (Fig. 2). Therefore, we suggest that downward percolation and subsequent accumulation is the dominant driving force for the heavy Li isotopic composition in the "regolith discontinuities" of both humid and arid regolith. Heavy δ^7Li signals in the deep saprolite units derived from meteoric water and clay-water partitioning from upper parts.

5.4. Li budget in shallow regolith

Our work presents a preliminary investigation of a series of regolith processes controlling Li elemental and isotopic signatures in the terrestrial weathering settings. As discussed above, Li geochemistry in the shallow regolith of the study area is impacted by basalt weathering, allochthonous deposition (dust, ash, and rainwater), and leaching in a state of approximate dynamic equilibrium. Although we are not able to directly determine the input and output fluxes of the regolith, we could use Li concentrations and its isotopic compositions to model the importance and contribution of these fluxes in soil horizons and compare weathering in wet and dry sites. We assume that mass input and output fluxes are identical if soil thickness is constant. Here, we built a simple isotopic mass-balance model for the shallow regolith, which has captured the loss and gain budgets of Li, to characterize leaching fluxes and primary mineral weathering contributions. Net Li mass gains (Δ_{Li}) relative to original basalt stock over 350 ka are identical to the difference between allochthonous Li inputs and the total Li outputs. Primary Li influxes include rainfall (F_{Rain}), Asian dust (F_{Dust}), rock weathering (F_{Wea}), and the principle output flux is leaching loss (F_{Leach}). We note that the possible contribution of ash is included in basalt weathering because of the similarity in isotopic compositions (Table S6). Since the deep regolith is often inaccessible to fine root tips, bio-lifting could be negligible, and not considered in our model setup in Eqs. (6) and (7):

$$\frac{dLi_{Soil}}{dt} = \Delta Li = F_{Rain} + F_{Dust} + F_{Wea} - F_{leach} \quad (6)$$

$$\begin{aligned}(\Delta Li \cdot \Delta^7 Li) = &\left(\left(F_{Rain} \cdot \delta^7 Li_{Rain}\right) + \left(F_{Dust} \cdot \delta^7 Li_{Dust}\right)\right. \\ &+ \left(F_{Wea} \cdot \delta^7 Li_{Basalt}\right) \\ &- \left(F_{Leach} \cdot \delta^7 Li_{Leach}\right)\end{aligned} \quad (7)$$

where Δ_{Li} is the net mass gain of Li in the shallow regolith; Δ^7Li is the isotopic composition of the net mass gain of Li, which is equal to the isotopic difference between the bulk soil and the parent rock. The absolute changes demonstrate the Li mass and isotopic offsets between primary and current materials as a function of input and output fluxes. In the above equations, F_X and $\delta^7 Li_X$ represent the values of accumulated Li fluxes over 350 ka and the constrained isotopic ratio of respective fluxes, respectively. The isotopic compositions of migrated dust, local rainfall, mineral weathering, and leach loss are obtained by direct measurement. Thus, the Li isotopic compositions of the shallow regolith are calculated using Eq. (8):

$$\delta^7 Li_{Shallowregolith} = \frac{\sum_{i=1}^{n} \delta^7 Li_i mLi_i}{\sum_{i=1}^{n} mLi_i} \quad (8)$$

where $\delta^7 Li_{Shallow\ regolith}$ is the mean isotopic composition of the total reservoir in the shallow regolith, $\delta^7 Li_i$ is the isotope composition of a measured layer (i) in the shallow regolith and mLi_i is the Li mass in layer (i). The rainfall Li inputs were calculated by Li concentration (0.15 ppb) in rainwater and geological time, and the dust Li inputs

were obtained by the product of quartz-based dust mass (Kurtz et al., 2001) and mean dust Li concentration (30.5 ug/g, the upper continental crust, Sauzéat et al., 2015). Fixed parameters include the Li isotopic compositions of the shallow regolith ($\delta^7Li_{Shallow\ regolith}$), dust ($\delta^7Li_{Dust}$), weathering ($\delta^7Li_{Wea}$), rainfall ($\delta^7Li_{Rain}$) and leach loss ($\delta^7Li_{Leach}$), and total Li inputs from rainfall (F_{Rain}) and dust (F_{Dust}) (Table S7). The weathering and leaching Li fluxes were calculated to achieve a balanced model by rearranging and solving the above equations (Fig. 8). Jackson et al. (1971) suggested that orographic rainfall in Hawaii efficiently washes dust out of trade wind clouds. We consider that increases in dust inputs with rainfall is reasonable since wet deposition potentially removes dust from the atmosphere. Our conclusion agrees with the interpretation of Parrington et al. (1983) that atmosphere transport and deposition of dust act as the condensation nuclei for raindrops. Increases in mineral weathering with rainfall are plausible, given weathering leaching becoming more intense driven by interstitial flows. Although marine aerosol flux in the arid site is small, the pattern of heavy Li isotopes may be reasoned by minor outputs by leaching. Water balance and associated pore water migration patterns are critical for Li geochemical behavior within the regolith. Such an interpretation is supported by a climate-driven threshold of 1400 mm·a^{-1} in the study area which has been evidenced by soil base cation storage (Chadwick et al., 2003), labile soil $^{87}Sr/^{86}Sr$ (Stewart et al., 2001) and meteoric ^{10}Be signals (Dixon et al., 2018).

5.5. Implications

The Li geochemical data of the humid and arid sites with those collected on the island of Hawaii along a climosequence of 150 ka age lava are shown in Fig. 9. Along the Hawaiian soil climosequence, depth-weighted average concentrations for Li with annual rainfalls up to 1,500 mm·a^{-1} are greater than these of parent lavas, and progressively became depleted after receiving greater annual rainfalls (Fig. 9a). The humid profile (BE) displays the most significant Li enrichment among all sampling sites, highlighting the importance of biological regulation (i.e., biolifting) for ~350 ka, in addition to atmospheric inputs. Another supportive evidence can be provided by higher Li enrichment levels in the arid profile (PO) compared to another site with similar annual rainfall but less development time. The conservation of Li in soils collapsed along at the sites receiving heavy rainfall over 2,000 mm. The Li isotopic composition of soils became heavy with annual rainfalls up to ~1,200 mm·a^{-1} and decreased with increasing rainfall

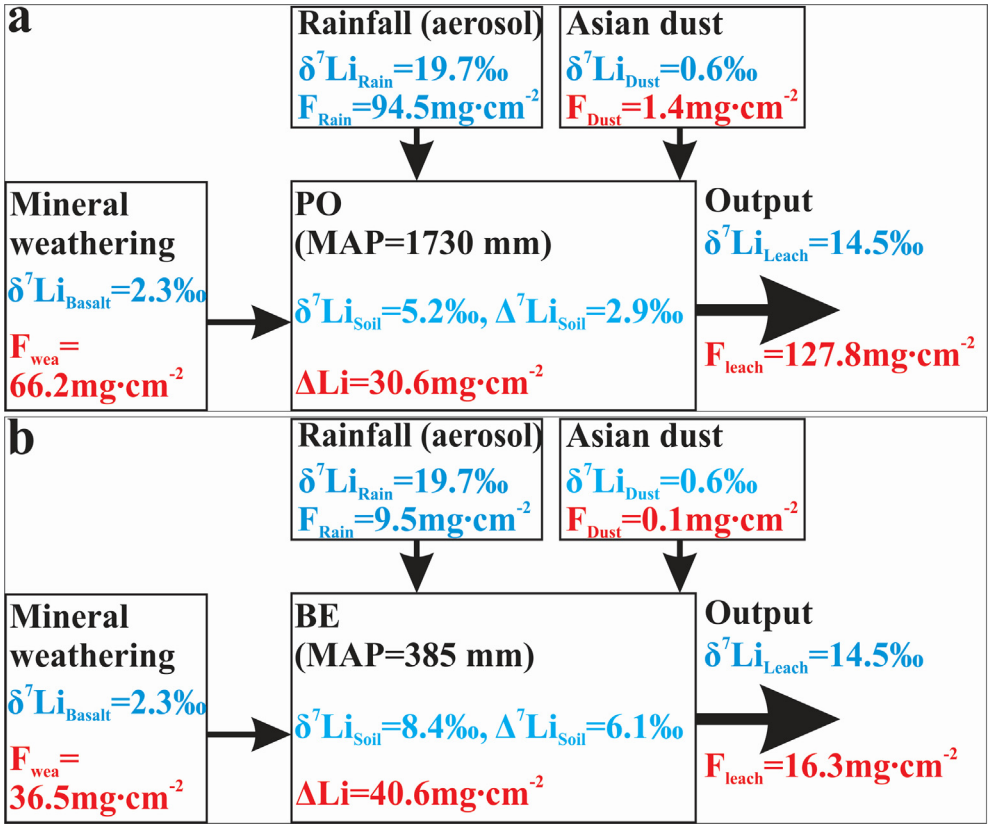

Fig. 8. Illustrations of box models of the Li budget in shallow regolith of (a) the humid regolith (MAP ~ 1730 mm) and (b) the arid regolith (MAP ~ 385 mm). Measured parameters are marked in blue and calculated parameters are marked in red. The volcanic ash input is included in mineral weathering. As the MAP increases, the contribution of atmospheric inputs increases. The leaching flux of Li increases with increasing rainfall and is generally enriched in heavy Li isotopes (δ^7Li_{Leach} = 14.6‰, equal to the mean value of groundwater). ^6Li is residually accumulated in soils (δ^7Li_{Humid} = 5.2‰, δ^7Li_{Arid} = 8.4‰. Mineral weathering and leaching fluxes were calculated using Eqs. (6) and (7).

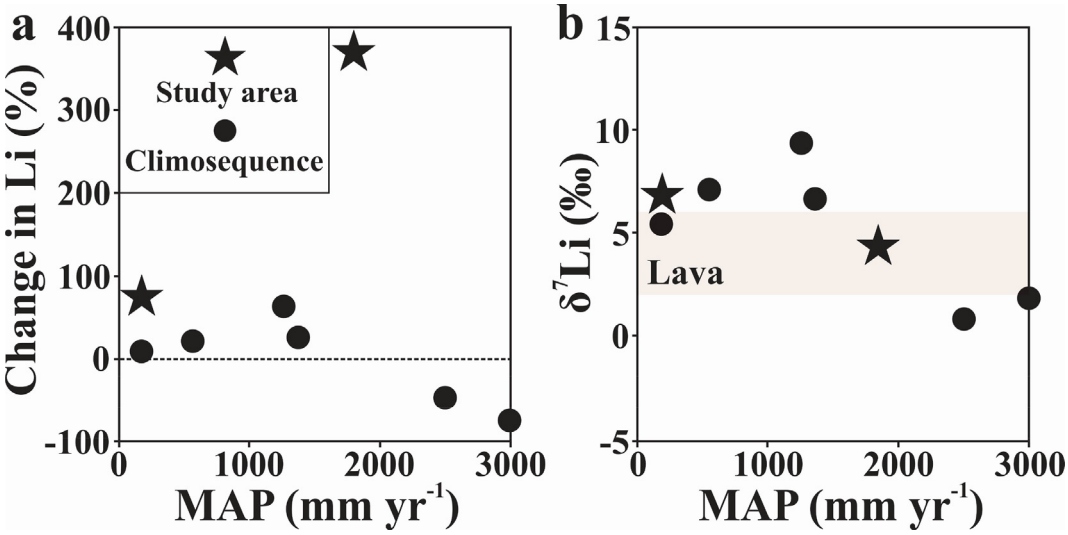

Fig. 9. Depth-integrated (a) soil Li loss and gain, and (b) soil δ^7Li across the Hawaiian climosequence (170 ka, Ryu et al., 2014) and the two regoliths (humid and arid, 350 ka, this study). The black circles represent the data of the climosequence sites at the age of ~150 ka. The stars represent the data of the study area (the humid and arid regoliths).

(Fig. 9b). Heavy isotopic compositions could be explained by the preservation of aerosol-derived signals in less humid environments (<1,500 mm·a^{-1}), while marine signals could be easily overprinted by rainwater in more humid conditions. In sum, our results highlight considerable climatic and biological controls on Li cycling in terrestrial settings.

Here, we compiled most reported Li elemental and isotopic data in weathered regoliths and fluvial sediments at global scales (Fig. 10). During continental weathering, the isotopically light Li is preferentially held by locally developed regolith through adsorption onto clay surfaces and incorporation into secondary clays (Pogge von Strandmann et al., 2008; Vigier et al., 2008; Millot et al., 2010a; Dellinger et al., 2015). Therefore, the Li transferred into river dissolved loads are isotopically heavy. In addition, as Li is further scavenged by secondary phases in fluvial sediments, river sediments become more Li-enriched and isotopically lighter from upper to lower reaches (Dellinger et al., 2015; Liu et al., 2015; Wang et al., 2015). Various processes (e.g., chemical weathering, diffusion, atmospheric addition and bio-interference) potentially result in the differentiation of Li isotopes in weathering products relative to the parent rock, depending on environmental conditions. For example, compiled data show that regoliths dispaly a wide range of Li concentrations from 0.4 to133 ug/g (Lemarchand et al., 2010; Liu et al., 2013) and δ^7Li from −20.2‰ to 26.7‰ (Rudnick et al., 2004; Pogge von Strandmann et al., 2012). Part of variabilities in Li geochemistry come from atmospheric addition of dusts, rainwaters, and marine aerosols (e.g., Pogge von Strandmann et al., 2012; Liu et al., 2013; Ryu et al., 2014). In addition, Li isotope fractionation driven

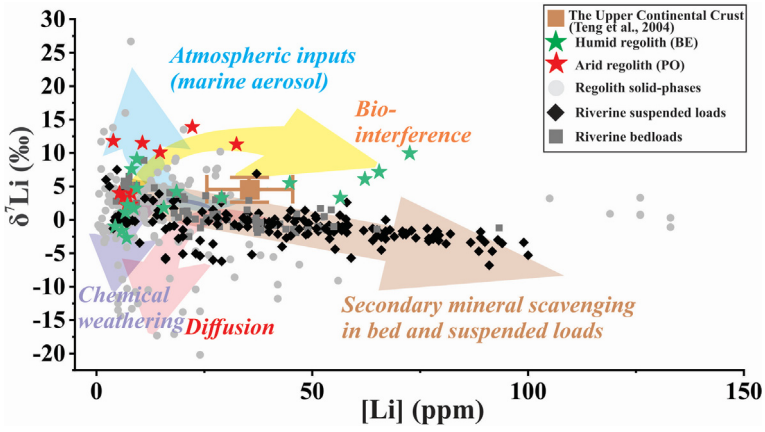

Fig. 10. The compilation of Li element concentration vs. isotopic composition in regolith profiles and river sediments (suspended and bed loads) at global scales (regolith: Clergue et al., 2015; Henchiri et al., 2016; Huh et al., 2004; Lemarchand et al., 2010; Liu et al., 2013; Pistiner and Henderson, 2003; Pogge von Strandmann et al., 2006; Rudnick et al., 2004; Ryu et al., 2014. River: Dellinger et al., 2015; Gou et al., 2019; Kisakürek et al., 2004; Liu et al., 2015; Romain Millot, Vigier, et al., 2010; Wang et al., 2015. See details in Fig. S6).

by diffusion along the pore water-filled grain-boundary may account for the extremely negative δ^7Li values in the scapolite (Teng et al., 2010). Particularly, we conclude that the biological influences emphasized in our study can be important in tropical forests, although further studies are needed. Given that, interpretations of Li isotopic composition in complex terrestrial environments require further considerations of sources and sinks, as well as controlling processes.

6. CONCLUSIONS

Our study provides detailed information on Li geochemistry in rocks, saprolites, soils, vegetation, and surrounding waters of the regolith profiles developed in the humid and arid sites of Hawaii. Compared with previous Hawaiian Li studies, our work highlights climate-regulated contribution to the Li cycle in the regolith. Therefore, δ^7Li signatures in the regolith should be treated with caution before using Li isotope system as a chemical weathering tracer. The Li geochemistry in the shallow regolith is mainly affected by atmospheric addition, vegetation cycling, and mineral synthesis, while it is controlled by pore fluid percolation and accumulation in the deep regolith. Dust input influences soil Li isotopic compositions in the humid site, and marine aerosol controls δ^7Li in soils from the arid site via secondary precipitation in equilibrium with temporal pore water. Continental dust and the ash inputs from recent Hawi eruptions (~150 ka) supports the Li enrichment in topsoils. The fidelity of biogeochemical cycling via biolifting resulted in peak Li accumulations in the rhizospheric soils, and light Li upward translocation as plant growth, and subsequently return into pore fluids by vegetative decay. Organic matter acts as an underestimated host of ^{6}Li in soils, which is supported by experimental humus-Li complexation. Biological activities greatly influence the humid site with dense plant covers. Secondary mineral formation and associated environments (e.g., mineral assemblages and pH) are also crucial for the retention, redistribution, and isotope fractionation of Li. The Li isotopic compositions in the deep regolith are similar to parent materials (the Pololu basalt), and downward infiltrative fluids generate accumulation zones (“regolith discontinuities”) in both sites. The result of this study emphasizes the climate and long-neglected biological controls on terrestrial Li cycling.

Declaration of Competing Interest

The authors declare that they have no known competing financial interests or personal relationships that could have appeared to influence the work reported in this paper.

ACKNOWLEDGEMENTS

We acknowledge funding support from the NSF Career Award (EAR1848153) and the University of North Carolina at Chapel Hill. The Sr isotope analysis was supported by the State Key Laboratory of Marine Geology, Tongji University (No. MGK1821). The manuscript benefited from the comments of the editor and three anonymous reviewers.

APPENDIX A. SUPPLEMENTARY MATERIAL

Supplementary data to this article can be found online at https://doi.org/10.1016/j.gca.2020.07.012.

REFERENCES

Anderson C. E. (1990) Lithium in plants. *In Lithium and Cell Physiology*. Springer, New York, NY.

Bagard M. L., Schmitt A. D., Chabaux F., Pokrovsky O. S., Viers J., Stille P., Labolle F. and Prokushkin A. S. (2013) Biogeochemistry of stable Ca and radiogenic Sr isotopes in a larch-covered permafrost-dominated watershed of Central Siberia. *Geochim. Cosmochim. Acta* **114**, 169–187.

Barker A. V. and Pilbeam D. J. (2016) *Handbook of plant nutrition*. CRC Press.

Bataille C. P., Willis A., Yang X. and Liu X. M. (2017) Continental igneous rock composition: A major control of past global chemical weathering. *Sci. Adv.*, 3.

Beaulieu E., Goddëris Y., Donnadieu Y., Labat D. and Roelandt C. (2012) High sensitivity of the continental-weathering carbon dioxide sink to future climate change. *Nat. Clim. Chang.* **2**, 346–349.

Blättler C. L., Jenkyns H. C., Reynard L. M. and Henderson G. M. (2011) Significant increases in global weathering during Oceanic Anoxic Events 1a and 2 indicated by calcium isotopes. *Earth Planet. Sci. Lett.* **309**, 77–88.

Brantley S. L. and White A. F. (2009) Approaches to modeling weathered regolith. *Rev. Mineral. Geochem.* **70**(1), 435–484. https://doi.org/10.2138/rmg.2009.70.10.

Bullen T. and Chadwick O. (2016) Ca, Sr and Ba stable isotopes reveal the fate of soil nutrients along a tropical climosequence in Hawaii. *Chem. Geol.* **422**, 25–45.

Chadwick O. A., Derry L. A., Vitousek P. M., Huebert B. J. and Hedin L. O. (1999) Changing sources of nutrients during four million years of ecosystem development. *Nature* **397**, 491–497.

Chadwick O. A., Gavenda R. T., Kelly E. F., Ziegler K., Olson C. G., Crawford E. W. and Hendricks D. M. (2003) The impact of climate on the biogeochemical functioning of volcanic soils. *Chem. Geol.* **202**, 195–223.

Chapela L. M., Buss H. L., Pogge von Strandmann P. A. E., Schuessler J. A. and Moore O. W. (2017) The influence of critical zone processes on the Mg isotope budget in a tropical, highly weathered andesitic catchment. *Geochim. Cosmochim. Acta* **202**, 77–100.

Clergue C., Dellinger M., Buss H. L., Gaillardet J., Benedetti M. F. and Dessert C. (2015) Influence of atmospheric deposits and secondary minerals on Li isotopes budget in a highly weathered catchment, Guadeloupe (Lesser Antilles). *Chem. Geol.* **414**, 28–41.

Dellinger M., Gaillardet J., Bouchez J., Calmels D., Louvat P., Dosseto A., Gorge C., Alanoca L. and Maurice L. (2015) Riverine Li isotope fractionation in the Amazon River basin controlled by the weathering regimes. *Geochim. Cosmochim. Acta* **164**, 71–93.

Dixon J. L., Chadwick O. A. and Pavich M. J. (2018) Climatically controlled delivery and retention of meteoric ^{10}Be in soils. *Geology* **46**, 899–902.

Fang Q., Hong H., Furnes H., Chorover J., Luo Q., Zhao L. and Algeo T. J. (2019) Surficial weathering of kaolin regolith in a subtropical climate: Implications for supergene pedogenesis and bedrock argillization. *Geoderma* **337**, 225–237.

Gaillardet J., Dupré B., Louvat P. and Allègre C. J. (1999) Global silicate weathering and CO_2 consumption rates deduced from the chemistry of large rivers. *Chem. Geol.* **159**, 3–30.

Georg R. B., Reynolds B. C., West A. J., Burton K. W. and Halliday A. N. (2007) Silicon isotope variations accompanying basalt weathering in Iceland. *Earth Planet. Sci. Lett.* **261**, 476–490.

Giambelluca T. W., Chen Q., Frazier A. G., Price J. P., Chen Y. L., Chu P. S., Eischeid J. K. and Delparte D. M. (2013) Online rainfall atlas of Hawai'i. *Bull. Am. Meteorol. Soc.* **94**, 313–316.

Gillaspy G. E., Keddie J. S., Oda K. and Gruissem W. (1995) Plant inositol monophosphatase is a lithium-sensitive enzyme encoded by a multigene family. *Plant Cell* **7**, 2175–2185.

Goodfellow B. W., Chadwick O. A. and Hilley G. E. (2014) Depth and character of rock weathering across a basaltic-hosted climosequence on Hawai'i. *Earth Surf. Process. Landforms* **39**, 381–398.

Gou L. F., Jin Z., Pogge von Strandmann P. A. E., Li G., Qu Y. X., Xiao J., Deng L. and Galy A. (2019) Li isotopes in the middle Yellow River: Seasonal variability, sources and fractionation. *Geochim. Cosmochim. Acta* **248**, 88–108.

Gupta N., Yadav K. K., Kumar V., Kumar S., Chadd R. P. and Kumar A. (2019) Trace elements in soil-vegetables interface: Translocation, bioaccumulation, toxicity and amelioration - A review. *Sci. Total Environ.* **651**, 2927–2942.

Hausrath E. M., Navarre-Sitchler A. K., Sak P. B., Williams J. Z. and Brantley S. L. (2011) Soil profiles as indicators of mineral weathering rates and organic interactions for a Pennsylvania diabase. *Chem. Geol.* **290**, 89–100.

Henchiri S., Gaillardet J., Dellinger M., Bouchez J. and Spencer R. G. M. (2016) Riverine dissolved lithium isotopic signatures in low-relief central Africa and their link to weathering regimes. *Geophys. Res. Lett.* **43**, 4391–4399.

Hess J., Bender M. L. and Schilling J. G. (1986) Evolution of the ratio of strontium-87 to strontium-86 in seawater from cretaceous to present. *Science* **231**, 979–984.

Hindshaw R. S., Tosca R., Goût T. L., Farnan I., Tosca N. J. and Tipper E. T. (2019) Experimental constraints on Li isotope fractionation during clay formation. *Geochim. Cosmochim. Acta* **250**, 219–237.

Hsieh J. C. C., Chadwick O. A., Kelly E. F. and Savin S. M. (1998) Oxygen isotopic composition of soil water: Quantifying evaporation and transpiration. *Geoderma* **82**, 269–293.

Huh Y., Chan L. H. and Chadwick O. A. (2004) Behavior of lithium and its isotopes during weathering of Hawaiian basalt. *Geochem., Geophys. Geosyst.*, 5.

Imseng M., Wiggenhauser M., Keller A., Müller M., Rehkämper M., Murphy K., Kreissig K., Frossard E., Wilcke W. and Bigalke M. (2018) Fate of Cd in agricultural soils: a stable isotope approach to anthropogenic impact, soil formation, and soil-plant cycling. *Environ. Sci. Technol.* **52**, 1919–1928.

Jackson M. L., Levelt T. W. M., Syers J. K., Rex R. W., Clayton R. N., Sherman G. D. and Uehara G. (1971) Geomorphological relationships of tropospherically derived quartz in the soils of the Hawaiian Islands. In pp. 515–525.

Jobbágy E. G. and Jackson R. B. (2001) The distribution of soil nutrients with depth: Global patterns and the imprint of plants. *Biogeochemistry* **53**, 51–77.

Kalinowska M., Hawrylak-Nowak B. and Szymańska M. (2013) The influence of two lithium forms on the growth, L-ascorbic acid content and lithium accumulation in lettuce plants. *Biol. Trace Elem. Res.* **152**, 251–257.

Kamber B. S., Greig A. and Collerson K. D. (2005) A new estimate for the composition of weathered young upper continental crust from alluvial sediments, Queensland, Australia. *Geochim. Cosmochim. Acta* **69**, 1041–1058.

Kasting J. F. and Catling D. (2003) Evolution of a habitable planet. *Annu. Rev. Astron. Astrophys.* **41**, 429–463.

Kimmig S. R., Holmden C. and Bélanger N. (2018) Biogeochemical cycling of Mg and its isotopes in a sugar maple forest in Québec. *Geochim. Cosmochim. Acta* **230**, 60–82.

Kisakürek B., Widdowson M. and James R. H. (2004) Behaviour of Li isotopes during continental weathering: The Bidar laterite profile, India. *Chem. Geol.* **212**, 27–44.

Kump L. R., Brantley S. L. and Arthur M. A. (2000) Chemical weathering, atmospheric CO2, and climate. *Annu. Rev. Earth Planet. Sci.* **28**, 611–667.

Kurtz A. C., Derry L. A. and Chadwick O. A. (2001) Accretion of Asian dust to Hawaiian soils: Isotopic, elemental, and mineral mass balances. *Geochim. Cosmochim. Acta* **65**, 1971–1983.

Lam P. J., Robinson L. F., Blusztajn J., Li C., Cook M. S., McManus J. F. and Keigwin L. D. (2013) Transient stratification as the cause of the North Pacific productivity spike during deglaciation. *Nat. Geosci.* **6**, 622–626.

Lemarchand E., Chabaux F., Vigier N., Millot R. and Pierret M. C. (2010) Lithium isotope systematics in a forested granitic catchment (Strengbach, Vosges Mountains, France). *Geochim. Cosmochim. Acta* **74**, 4612–4628.

Li W. and Liu X. M. (2020) Experimental determination of lithium isotopic fractionation during clay adsorption: Implications for chemical weathering. *Geochim. Cosmochim. Acta* **284**, 156–172.

Li G. and West A. J. (2014) Evolution of Cenozoic seawater lithium isotopes: Coupling of global denudation regime and shifting seawater sinks. *Earth Planet. Sci. Lett.* **401**, 284–293.

Li W., Liu X. M. and Godfrey L. V. (2019) Optimisation of lithium chromatography for isotopic analysis in geological reference materials by MC-ICP-MS. *Geostand. Geoanal. Res.* **43**, 261–276.

Liu H. C., You C. F., Huang K. F. and Chung C. H. (2012) Precise determination of triple Sr isotopes (δ^{87}Sr and δ^{88}Sr) using MC-ICP-MS. *Talanta* **88**, 338–344.

Liu X. M. and Li W. (2019) Optimization of lithium isotope analysis in geological materials by quadrupole ICP-MS. *J. Anal. At. Spectrom.* **34**, 1708–1717.

Liu X. M. and Rudnick R. L. (2011) Constraints on continental crustal mass loss via chemical weathering using lithium and its isotopes. *Proc. Natl. Acad. Sci. U. S. A.* **108**, 20873–20880.

Liu X. M., Rudnick R. L., McDonough W. F. and Cummings M. L. (2013) Influence of chemical weathering on the composition of the continental crust: Insights from Li and Nd isotopes in bauxite profiles developed on Columbia River Basalts. *Geochim. Cosmochim. Acta* **115**, 73–91.

Liu X. M., Teng F. Z., Rudnick R. L., McDonough W. F. and Cummings M. L. (2014) Massive magnesium depletion and isotope fractionation in weathered basalts. *Geochim. Cosmochim. Acta* **135**, 336–349.

Liu X. M., Wanner C., Rudnick R. L. and McDonough W. F. (2015) Processes controlling δ^7Li in rivers illuminated by study of streams and groundwaters draining basalts. *Earth Planet. Sci. Lett.* **409**, 212–224.

Millot R. and Girard J. P. (2007) Lithium isotope fractionation during adsorption onto mineral surfaces. Clays Nat. Eng. Barriers Radioact. Waste Confin. 3rd Int. Meet., 307–308. Available at: http://www.andra.fr/lille2007/abstract_lille2007/donnees/pdf/307_308_P_GM_6.pdf.

Millot R., Petelet-Giraud E., Guerrot C. and Négrel P. (2010a) Multi-isotopic composition (δ^7Li-δ^{11}B-δD-δ^{18}O) of rainwaters in France: Origin and spatio-temporal characterization. *Appl. Geochem.* **25**, 1510–1524.

Millot R., Vigier N. and Gaillardet J. (2010b) Behaviour of lithium and its isotopes during weathering in the Mackenzie Basin, Canada. *Geochim. Cosmochim. Acta* **74**, 3897–3912.

Misra S. and Froelich P. N. (2012) Lithium isotope history of cenozoic seawater: Changes in silicate weathering and reverse weathering. *Science* **335**, 818–823.

Murphy M. J., Porcelli D., Pogge von Strandmann P. A. E., Hirst C. A., Kutscher L., Katchinoff J. A., Mörth C. M., Maximov T. and Andersson P. S. (2019) Tracing silicate weathering processes in the permafrost-dominated Lena River watershed using lithium isotopes. *Geochim. Cosmochim. Acta* **245**, 154–171.

Opfergelt S., Burton K. W., Georg R. B., West A. J., Guicharnaud R. A., Sigfusson B., Siebert C., Gislason S. R. and Halliday A. N. (2014) Magnesium retention on the soil exchange complex controlling Mg isotope variations in soils, soil solutions and vegetation in volcanic soils, Iceland. *Geochim. Cosmochim. Acta* **125**, 110–130.

Palumbo B., Angelone M., Bellanca A., Dazzi C., Hauser S., Neri R. and Wilson J. (2000) Influence of inheritance and pedogenesis on heavy metal distribution in soils of Sicily, Italy. *Geoderma* **95**, 247–266.

Parrington J. R., Zoller W. H. and Aras N. K. (1983) Asian dust: Seasonal transport to the Hawaiian Islands. *Science* **220**, 195–197.

Penniston-Dorland S., Liu X. M. and Rudnick R. L. (2017) Lithium isotope geochemistry. *Non-Traditional Stable Isotopes Walter de Gruyter GmbH.*, 165–218.

Pistiner J. S. and Henderson G. M. (2003) Lithium-isotope fractionation during continental weathering processes. *Earth Planet. Sci. Lett.* **214**, 327–339.

Pogge von Strandmann P. A. E., Burton K. W., James R. H., van Calsteren P., Gíslason S. R. and Mokadem F. (2006) Riverine behaviour of uranium and lithium isotopes in an actively glaciated basaltic terrain. *Earth Planet. Sci. Lett.* **251**, 134–147.

Pogge von Strandmann P. A. E., Burton K. W., James R. H., van Calsteren P. and Gislason S. R. (2010) Assessing the role of climate on uranium and lithium isotope behaviour in rivers draining a basaltic terrain. *Chem. Geol.* **270**, 227–239.

Pogge von Strandmann P. A. E., Fraser W. T., Hammond S. J., Tarbuck G., Wood I. G., Oelkers E. H. and Murphy M. J. (2019) Experimental determination of Li isotope behaviour during basalt weathering. *Chem. Geol.* **517**, 34–43.

Pogge von Strandmann P. A. E. and Henderson G. M. (2015) The Li isotope response to mountain uplift. *Geology* **43**, 67–70.

Pogge von Strandmann P. A. E., James R. H., van Calsteren P., Gíslason S. R. and Burton K. W. (2008) Lithium, magnesium and uranium isotope behaviour in the estuarine environment of basaltic islands. *Earth Planet. Sci. Lett.* **274**, 462–471.

Pogge Von Strandmann P. A. E., Jenkyns H. C. and Woodfine R. G. (2013) Lithium isotope evidence for enhanced weathering during Oceanic Anoxic Event 2. *Nat. Geosci.* **6**, 668–672.

Pogge von Strandmann P. A. E., Opfergelt S., Lai Y. J., Sigfússon B., Gislason S. R. and Burton K. W. (2012) Lithium, magnesium and silicon isotope behaviour accompanying weathering in a basaltic soil and pore water profile in Iceland. *Earth Planet. Sci. Lett.* **339–340**, 11–23.

Porder S., Hilley G. E. and Chadwick O. A. (2007) Chemical weathering, mass loss, and dust inputs across a climate by time matrix in the Hawaiian Islands. *Earth Planet. Sci. Lett.* **258**, 414–427.

Putra A. R., Tachibana Y., Tanaka M. and Suzuki T. (2018) Lithium isotope separation using displacement chromatography by cation exchange resin with high degree of cross-linkage. *Fusion Eng. Des.* **136**, 377–380.

Raczek I., Jochum K. P. and Hofmann A. W. (2001) Neodymium and strontium isotope data for USGS reference GSP-1, GSP-2 and eight MPI-DING reference glasses Available at:. *Geostand. Newsletterthe J. Geostand. Geoanal.* **27**, 173–179 http://www3.interscience.wiley.com/journal/119925531/abstract.

Reimann C., Englmaier P., Flem B., Gough L., Lamothe P., Nordgulen and Smith D. (2009) Geochemical gradients in soil O-horizon samples from southern Norway: Natural or anthropogenic? *Appl. Geochem.* **24**, 62–76.

Robinson B. H., Yalamanchali R., Reiser R. and Dickinson N. M. (2018) Lithium as an emerging environmental contaminant: Mobility in the soil-plant system. *Chemosphere* **197**, 1–6.

Rudnick R. L., Tomascak P. B., Njo H. B. and Gardner L. R. (2004) Extreme lithium isotope fractionation during continental weathering revealed in saprolites from South Carolina. *Chem. Geol.* **212**, 45–57.

Ryu J. S., Vigier N., Lee S. W., Lee K. S. and Chadwick O. A. (2014) Variation of lithium isotope geochemistry during basalt weathering and secondary mineral transformations in Hawaii. *Geochim. Cosmochim. Acta* **145**, 103–115.

Sauzéat L., Rudnick R. L., Chauvel C., Garçon M. and Tang M. (2015) New perspectives on the Li isotopic composition of the upper continental crust and its weathering signature. *Earth Planet. Sci. Lett.* **428**, 181–192.

Shahzad B., Tanveer M., Hassan W., Shah A. N., Anjum S. A., Cheema S. A. and Ali I. (2016) Lithium toxicity in plants: Reasons, mechanisms and remediation possibilities – A review. *Plant Physiol. Biochem.* **107**, 104–115.

Spengler S. R. and Garcia M. O. (1988) Geochemistry of the Hawi lavas, Kohala Volcano, Hawaii. *Contrib. Mineral. Petrol.* **99**, 90–104.

Stewart B. W., Capo R. C. and Chadwick O. A. (2001) Effects of rainfall on weathering rate, base cation provenance, and Sr isotope composition of Hawaiian soils. *Geochim. Cosmochim. Acta* **65**, 1087–1099.

Stille P., Pierret M. C., Steinmann M., Chabaux F., Boutin R., Aubert D., Pourcelot L. and Morvan G. (2009) Impact of atmospheric deposition, biogeochemical cycling and water-mineral interaction on REE fractionation in acidic surface soils and soil water (the Strengbach case). *Chem. Geol.* **264**, 173–186.

Teng F. Z., Li W. Y., Rudnick R. L. and Gardner L. R. (2010) Contrasting lithium and magnesium isotope fractionation during continental weathering. *Earth Planet. Sci. Lett.* **300**, 63–71.

Tomascak P. B. (2004) Developments in the understanding and application of lithium isotopes in the Earth and planetary sciences. *Rev. Mineral. Geochem.* **55**, 153–195.

Vigier N., Decarreau A., Millot R., Carignan J., Petit S. and France-Lanord C. (2008) Quantifying Li isotope fractionation during smectite formation and implications for the Li cycle. *Geochim. Cosmochim. Acta* **72**, 780–792.

Vigier N., Gislason S. R., Burton K. W., Millot R. and Mokadem F. (2009) The relationship between riverine lithium isotope composition and silicate weathering rates in Iceland. *Earth Planet. Sci. Lett.* **287**, 434–441.

Vigier N. and Goddéris Y. (2015) A new approach for modeling Cenozoic oceanic lithium isotope paleo-variations: The key role of climate. *Clim. Past* **11**, 635–645.

Wang Q. L., Chetelat B., Zhao Z. Q., Ding H., Li S. L., Wang B. L., Li J. and Liu X. L. (2015) Behavior of lithium isotopes in the Changjiang River system: Sources effects and response to weathering and erosion. *Geochim. Cosmochim. Acta* **151**, 117–132.

Wanner C., Sonnenthal E. L. and Liu X. M. (2014) Seawater δ^7Li: A direct proxy for global CO_2 consumption by continental silicate weathering? *Chem. Geol.* **381**, 154–167.

Whipkey C. E., Capo R. C., Chadwick O. A. and Stewart B. W. (2000) The importance of sea spray to the cation budget of a

coastal Hawaiian soil: A strontium isotope approach. *Chem. Geol.* **168**, 37–48.

White A. F., Schulz M. S., Stonestrom D. A., Vivit D. V., Fitzpatrick J., Bullen T. D., Maher K. and Blum A. E. (2009) Chemical weathering of a marine terrace chronosequence, Santa Cruz, California. Part II: Solute profiles, gradients and the comparisons of contemporary and long-term weathering rates. *Geochim. Cosmochim. Acta* **73**, 2769–2803.

Wiegand B. A., Chadwick O. A., Vitousek P. M. and Wooden J. L. (2005) Ca cycling and isotopic fluxes in forested ecosystems in Hawaii. *Geophys. Res. Lett.* **32**, 1–4.

Zhang L., Chan L. H. and Gieskes J. M. (1998) Lithium isotope geochemistry of pore waters from Ocean Drilling Program Sites 918 and 919, irminger basin. *Geochim. Cosmochim. Acta* **62**, 2437–2450.

Zhang S., Yuan L., Li W., Lin Z., Li Y., Hu S. and Zhao B. (2017) Characterization of pH-fractionated humic acids derived from Chinese weathered coal. *Chemosphere* **166**, 334–342.

Ziegler K., Hsieh J. C. C., Chadwick O. A., Kelly E. F., Hendricks D. M. and Savine S. M. (2003) Halloysite as a kinetically controlled end product of arid-zone basalt weathering. *Chem. Geol.* **202**, 461–478.

Associate editor: Brian W. Stewart